DRA

NASA CR- 177825

A Study of Eddy-Mean Flow Interactions Using Eliassen-Palm Diagnostics: FGGE SOP-1 Data and the NASA GLAS General Circulation Model Compared

Mark P. Baldwin
H. J. Edmon, Jr.
James R. Holton

Department of Atmospheric Sciences
University of Washington
Seattle, WA 98195

FINAL TECHNICAL REPORT
NASA Grant NAG5-233
"Diagnostic Studies of the Atmospheric Circulation"
James R. Holton, Principal Investigator
Grant Period: April 1982 - March 1984

ABSTRACT

Latitude-height cross sections of the Eliassen-Palm (EP) flux, its divergence, the residual mean meridional circulation, as well as convential eddy and mean flow fields are computed using both observational and general circulation model data.

Two month average cross sections for both stationary and transient eddy statistics are displayed for the FGGE Special Observing Period 1 (SOP-1) and for an analogous two month simulation from the GLAS general circulation model. EP cross sections for FGGE SOP-1 are in good agreement with cross sections computed using Oort's 11-year mean Northern Hemisphere winter climatology. Exceptions are in the Northern Hemisphere tropical upper troposphere and high latitude stratosphere where anomalously large poleward transient eddy heat fluxes occur in the FGGE SOP-1 data.

EP cross sections from the GLAS Model differ markedly from those computed with atmospheric data. Some of these differences are probably associated with the anomalous high latitude location of the winter jetstream in the GLAS model. The most unusual feature of the GLAS Model is that the maximum amplitude of the mid-latitude heat flux is at 1000 mb. Thus, the vertical gradient of the lower troposphere heat flux is opposite that in the atmosphere.

Time series of the daily EP flux divergence are compared to the mean zonal wind accelerations. The EP flux divergence is generally strongly compensated by the Coriolis torque of the residual mean meridional circulation. The sum of these is poorly correlated with zonal flow acceleration in the FGGE data, but somewhat better correlated in the GLAS model data. In general the EP flux divergence is not a useful measure of mean flow acceleration.

1. Introduction

Edmon et al. (1980) showed that latitude height cross sections of the so called Eliassen Palm (EP) flux and its divergence provide very useful diagnostics for understanding the interaction between zonally asymmetric "eddy" disturbances and the zonal mean circulation. To quote from their paper:

> "Such EP cross sections exhibit the principal eddy heat, momentum and potential vorticity fluxes in one diagram, making their relative magnitudes and spatial relationships easier to appreciate. They provide a succinct framework for comparing theory, observation, and numerical experiment, and for assessing parameterizations of eddy effects. Moreover, the particular combinations of eddy fluxes which are represented on an EP cross section are fundamental for the interaction between eddies and the mean state, more so than the eddy heat and momentum fluxes considered separately, and more so than the eddy energy fluxes originally emphasized by Eliassen and Palm themselves."

The theory of eddy forcing of the zonal mean circulation has been discussed by Andrews and McIntyre (1976), Holton (1980), Dunkerton et al. (1981) and others. In these papers it is shown that net eddy forcing can be expressed in terms of the northward flux of quasi-geostrophic potential vorticity (which turns out to equal the divergence of the EP flux). Furthermore, for steady conservative linear waves the EP flux divergence vanishes so that there is no net mean flow forcing by the eddies even though eddy heat and momentum fluxes may individually be very large! This apparent paradox can be explained by the compensating effect of the mean meridional

circulation driven by the eddies which serves, through the Coriolis force and adiabatic cooling/heating, to cancel the momentum and thermal forcing by the eddies. Thus, whereas patterns of eddy momentum and heat flux divergences in themselves give very little information on eddy-mean flow interaction, patterns of EP flux divergence should provide very useful diagnostics of the interaction process.

In Edmon et al., the EP flux cross sections were computed for two sets of Northern Hemisphere data: Oort and Rasmussen's (1971) station data from 10°S to 70°N latitude 1958-1963, and NMC gridded data from 20°N to 90°N latitude for the years 1965-1977. For the NMC data set EP flux statistics were computed from 120 day winter mean and 120 day summer mean data while the Oort and Rasmussen data set used 90 day means. For each of the samples EP flux cross sections were calculated separately for transient eddies and stationary (120 or 90 day time averaged) eddies.

The flux patterns are similar for the two data sets in winter, but less so in summer. Whether the differences are a result of data inadequacies or real climate differences between the two periods is not known. By comparing the observed cross sections with cross sections derived from model calculations Edmon et al. showed that the observed fluxes are consistent with the fluxes due to nonlinear baroclinic waves averaged over the life cycles of the waves, but are not consistent with linear baroclinic instability theory.

Due to the limitations of the data sets used in Edmon et al. (e.g., geographical bias, incomplete latitudinal coverage, deficient analysis scheme at 1000 mb in the NMC data, etc.) it is clear that further studies with a more

complete <u>global</u> data set should be carried out. In addition, EP flux cross sections should be computed for a state of the art general circulation model to provide an additional diagnostic for model validation and for elucidating various physical processes.

As a contribution to these objectives we here report EP diagnostics for two data sets: The FGGE SOP-1 data and a two month (Northern winter) simulation with the Goddard Laboratory for Atmospheric Sciences (GLAS) general circulation model.

2. Theoretical Background

Most of the relevant theory is given in Edmon <u>et al</u>. (1980) and Palmer (1981). In log-pressure coordinates, the zonal mean equations are

$$(1)\quad \frac{\partial \bar{u}}{\partial t} = f\bar{v} - \frac{1}{r\cos^2\phi}\frac{\partial}{\partial\phi}(\cos^2\phi\ \overline{u'v'})$$

$$(2)\quad \frac{\partial \bar{\theta}}{\partial t} = -\frac{\bar{\theta}_\phi \bar{v}}{r_0} - \bar{\theta}_z\bar{w} - \frac{1}{r_0\cos\theta}\frac{\partial}{\partial\phi}(\cos\theta\ \overline{v'\theta'}) + \bar{Q}$$

where

$$(3)\quad z = -H \ln(P/1000 \text{ mb})$$

and other notation follows Palmer (1981), if we define a "residual" mean meridional circulation (v^*, w^*) by letting

$$(4)\quad \bar{v}^* \equiv \bar{v} - e^{z/H}\frac{\partial}{\partial z}\left(e^{-z/H}\frac{\overline{v'\theta'}}{\bar{\theta}_z}\right)$$

$$(5)\quad \overline{w}^* \equiv \overline{w} + \frac{1}{r_0 \cos\theta}\frac{\partial}{\partial\phi}\left(\cos\theta\, \frac{\overline{v'\theta'}}{\overline{\theta}_z}\right)$$

the zonal mean equations may then be written in the transformed Eulerian mean form as:

$$(6)\quad \frac{\partial\overline{u}}{\partial t} - f\overline{v}^* - G = \nabla\cdot\mathbf{F}/(r_0\cos\theta\, e^{z/H})$$

$$(7)\quad \frac{\partial\overline{\theta}}{\partial t} = -\overline{\theta}_z\overline{w}^* - \frac{\overline{\theta}_\phi\overline{v}^*}{r_0} - \frac{1}{r_0\cos\theta}\frac{\partial}{\partial\phi}\left(\cos\phi\, \overline{v'\theta'}\right) + \overline{Q}$$

with

$$(8)\quad \mathbf{F} = r_0\cos\phi\, e^{-z/H}\left(-\overline{u'v'},\ f\frac{\overline{v'\theta'}}{\overline{\theta}_z}\right)$$

and G denotes the drag force due to unresolved eddies. Thus, divergence of the EP flux (scaled by $(r_0 \cos\phi)^{-1}\exp(-z/H)$ is the sole forcing of the mean flow by the meteorological eddies. If $\nabla\cdot\mathbf{F}$, $\overline{Q}$ and G all vanish, thus a steady state is possible (Charney and Drazin, 1961).

Divergence of the EP flux also gives the northward transport of quasi-geostrophic potential vorticity. Palmer (1982) has shown that in spherical coordinates this relationship has the form:

$$(9)\quad \overline{v'q'}_{(m)} = \nabla\cdot\mathbf{F}\,(r_0\cos\phi\, e^{-z/H})$$

where q'(m) is a modified eddy quasi-geostrophic potential vorticity given by:

$$(10)\quad q'_{(m)} = v'_x - \frac{f}{\cos\phi}\left(\frac{\cos\phi}{f}u'\right)_y + f\left[\frac{\theta'}{\overline{\theta}_z}e^{-z/H}\right]$$

The EP flux is also important in wave theory. A conservation relation of the form

$$(11)\quad \frac{\partial A}{\partial t} + \nabla\cdot\mathbf{F}\,(r\cos\theta\, e^{-z/H}) = D$$

was derived by Andrews and McIntyre (1976, 1978). See Strauss (1983) for a review of this subject. D is zero for conservative motion and A can be called the EP wave activity

$$(12)\quad A \approx \frac{1}{2}\,(\overline{q'})^2 \,/\, \overline{q}_y$$

For planetary scale waves for which WKBJ theory holds,

$$(13)\quad \mathbf{F} \approx \mathbf{C}_g\, A$$

where $\mathbf{C}_g$ is the group velocity of the waves. Thus, within these approximations, wave energy will propagate parallel to $\mathbf{F}$.

The streamfunction for the residual mean meridional circulation is given by

$$(14)\quad \bar{v}^* = -\frac{g}{2\pi r_0^{\,2} p_0 \cos\phi}\,\frac{\partial\bar{\psi}^*}{\partial z}$$

$$(15)\quad \bar{w}^* = \frac{g}{2\pi r_0^{\,2} p_0 \cos\phi}\,\frac{\partial\bar{\psi}^*}{\partial\phi}$$

A single convention for plotting EP cross sections has not yet emerged. The EP diagrams shown here differ somewhat from those is Edmon _et al._ (1980). The diagrams here use log p as a vertical coordinate. Edmon _et al._ plotted a modified EP flux divergence (see their equations 3.10 to 3.13). The quantity plotted here is

$$(16) \quad \nabla \cdot \mathbf{F} \; / \; \left[r_0 \cos \phi \; e^{-z/H}\right]$$

which clearly shows the net driving force by the eddies on the mean flow with contours in ms^{-1} day^{-1}.

Edmon et al. have plotted $\mathbf{F}$ (y,p) scaled so that the arrows appear divergent when $\nabla \cdot \mathbf{F} > 0$. This scaling inevitably emphasises the lower troposphere. This is due to the factor exp (-z/H) contained in $\mathbf{F}$. A sensible compromise is to leave out the factor of exp (-z/H) when plotting $\mathbf{F}$. This results in arrows of similar lengths everywhere in the diagram, for similar heat and momentum fluxes. The only information altered is the magnitude of the group velocity of the waves, which isn't easily obtained from the diagrams. This plotting convention retains the magnitudes of the heat and momentum fluxes, which is a significant advantage.

In deriving the approximate thermodynamic energy equation, the assumption that the static stability is independent of latitude is generally made. The latitudinally varying part of the static stability must be neglected in order that the thermodynamic energy equation contain no eddy flux terms.

This assumption is not needed in deriving the zonal mean quasi-geostrophic thermodynamic energy equation if the equations are to be used to diagnose the wave driving of the mean wind.

In deriving (6) and (7), the residual mean meridional velocity (4) is substituted into (1) and (2). The assumption is made that

$$(17) \quad \frac{\partial}{\partial \phi}(\cos \phi \; \overline{v'\theta'}) = \overline{\theta}_z \frac{\partial}{\partial \phi}\left[\cos \phi \; \frac{\overline{v'\theta'}}{\overline{\theta}_z}\right],$$

which assumes that $\overline{\theta}_z$ does not vary with latitude. This assumption is necessary in order to derive the Eliassen-Palm theorem for arbitrary eddy amplitudes (Stone and Salustri, 1984).

However, if the transformed Eulerian mean equations are to be used to diagnose eddy forcing of the zonal mean wind, it is incorrect to restrict the latitudinal variation of θ_z. Both the results shown here and those of Edmon et al. were calculated with the variable stability.

The restriction to a stability dependent on height only would cause large changes in the EP flux and its divergence. For example, the static stability at 200 mb is about five times as great at 60°N as it is at 20°N.

The usual formulation of the EP flux neglects the effects of moisture and friction. Stone and Salustri (1984) have argued that the EP flux should include all the effects of the eddies, both explicit and implicit which force the mean wind. They have shown that a term

$$(p_0/p)^{R/Cp}\,(L/Cp)\,(\overline{v'q'})$$

should be added to the heat flux, $\overline{v'\theta'}$, to account for the eddy moisture flux. However, their formulation requires a static stability that is independent of latitude, which would cause large changes in the EP flux, as discussed above. Since the eddy moisture flux is confined to the lower troposphere, "moist" EP flux results were calculated using the variable static stability. This will give a better representation of the eddy forcing of the mean wind.

Stone and Salustri have also suggested using a modified static stability

$$(18) \quad \sigma_m = \frac{\partial \overline{\theta}}{\partial p} + \frac{L}{Cp}\left[\frac{p_0}{p}\right]^{R/Cp}\frac{\partial q}{\partial p}$$

The conditionally unstable tropical atmosphere is unstable by this definition. The use of this stability would result in very large vertical EP flux components in region where $\sigma_m \approx 0$. The result would be a very erratic pattern in the tropical lower troposphere.

Since, on the average, the tropical atmosphere is not saturated, it is more appropriate to use the usual dry static stability, but include the effect of moisture by using virtual potential temperature instead of potential temperature. The use of

$$(19) \quad \sigma_m = \frac{\partial \theta_v}{\partial p}$$

would only make a small difference in the vertical EP flux component, since the difference between θ_v and θ is small.

3. Description of the data and analysis

The Oort (1983) atmospheric statistics serve as a standard climatology to compare with both two-month data sets. Edmon et al. used the Oort and Rasmusson (1971) statistics for some of their calculations. That data set covered the latitudes from 40°S to 80°N and used eight years of station data (1958-1963). The Oort statistics used 11 years of station data (1963-1973) and covered both hemispheres, from 80°S to 80°N.

Before discussion of the EP diagrams, the FGGE data and the GLAS model data will be compared to the Oort climatology using conventional climate statistics.

Comparisons will be made for both transient and stationary eddy statistics. It is important to note that the Oort transient wave statistics are defined as deviations from December - February (90 day) averages, while the averaging period for both the FGGE analysis and the GLAS model data is 58 days. Thus, part of what appears in the stationary waves in the FGGE or GLAS model data would appear in the transient eddies in the Oort analysis. However, this difference is probably small in most cases.

The Oort statistics are probably the best representation of the zonal mean climatology available. A comparison between the FGGE data and the Oort statistics should reveal how the FGGE SOP-1 differed from the climatological average. It is also possible that the high quality of the FGGE SOP-1 data will allow some features to be discerned that were not captured in the Oort analysis.

Similarly, a comparison between the GLAS model data and the Oort statistics should reveal how the model differs from climatology. Of course, some features in the model will be due to averaging over only one model winter. The main objective of this study is to compare EP flux diagrams for the GLAS model, the FGGE SOP-1 data and the Oort climatology. These comparisons include, for the FGGE and GLAS model data, not only two-month means but five-day means and even one-day means.

a) The FGGE SOP-1 data

The data set consists of the FGGE analysis for SOP-1, January 4 - March 2, 1979 from Goddard Space Flight Center analyses

(Experiments number 2254, 2274 and 2282). The data were available at 0000 CMT and 1200 CMT daily on a 4° latitude by 5° latitude grid (46x72) that covered the entire globe. The data were available at the twelve standard pressure levels from 1000 to 50 mb (1000, 850, 700, 500, 400, 300, 250, 200, 150, 100, 70, 50 mb). The following quantities were available, u and v wind components, ω vertical velocity, temperature, geopotential height, relative humidity and diabatic heating. It is expected that the FGGE SOP-1 data set, because of the large number of observations available, is an excellent representation of the atmosphere during that period. However, it is important to determine how close the FGGE winter was to the climatological norm. Any differences could be either actual differences between the FGGE winter and the average, or could be features missed in the normal meteorological analysis.

b) The GLAS model data

The GLAS model is a grid point primitive equation model with a horizontal resolution of 4° latitude by 5° longitude. The pressure levels are the same as for the FGGE data set, except that the highest level in the model is 70 mb instead of 50 mb. The levels for the data set are 1000, 850, 700, 500, 400, 300, 250, 200, 150 and 100 mb. The 70 mb level was not available.

The only fields available were u and v wind components, ω vertical velocity, temperature and geopotential height.

The model was initialized with real atmospheric data from January 1, 1975. As with the FGGE data, 58 days were used in the analysis.

4. FGGE SOP-1 results

a) Zonal mean fields - Comparison with Oort data set.

Each of the zonal mean fields, covering from 90°S to 90°N is displayed with the equivalent Oort (1983) figures. Note that the Oort analysis stops at 80°S and 80°N. Following these, we also present the same fields, but for the equator to 80°N, in order to facilitate comparison with the EP diagrams which also extend from the equator to 80°N.

The zonal component of the wind (Fig. 1A) is very similar to the Oort climatology (Fig. 2A). The location and strength of the northern hemisphere jet are nearly the same, while the southern hemisphere jet is slightly stronger and about 5° farther south than normal.

The most striking difference is the lack of easterlies between 200 and 500 mb in the tropics. This indicates that the FGGE year differed from climatology in the tropics.

The meridional wind component (Fig. 1B) is fairly representative of climatology. The main difference is that the northern hemisphere Ferrel cell circulation is not as clear as in the Oort data. The

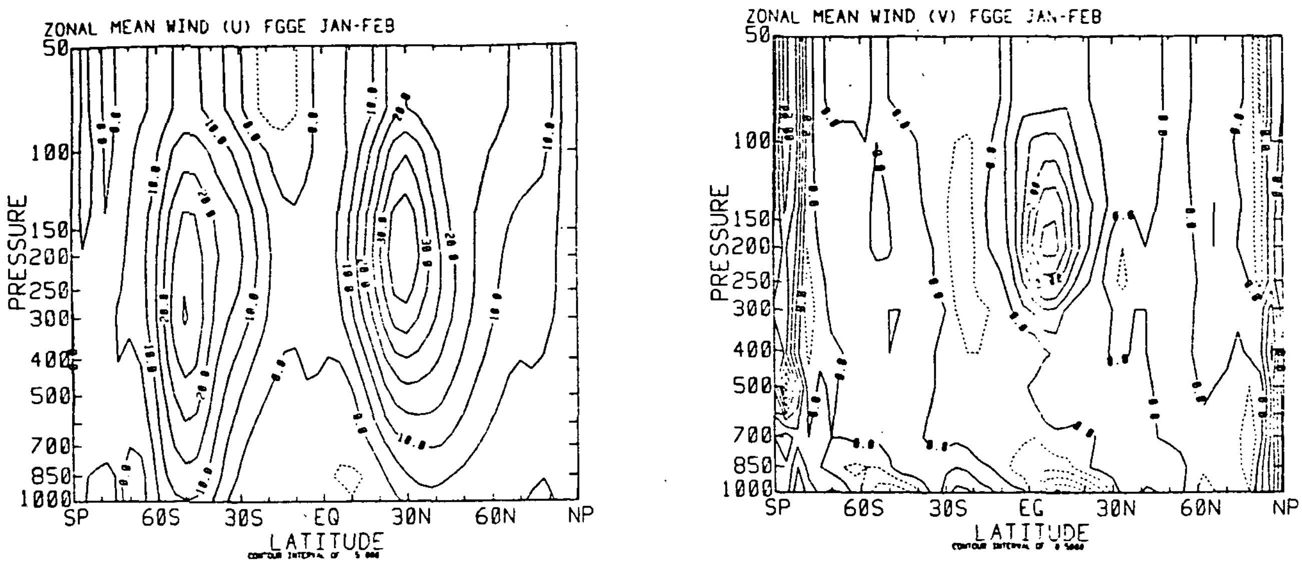

Fig. 1. Zonal mean u and v wind components for FGGE data

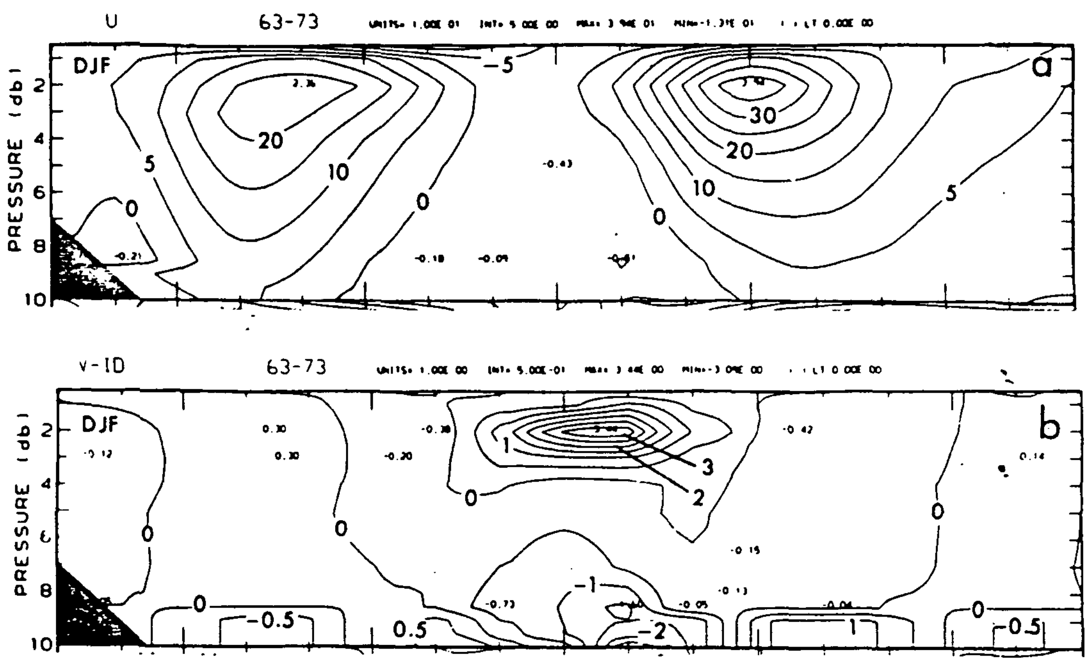

Fig. 2. Zonal mean u and v wind components for 11 years of winter data. (From Oort, 1983)

northern hemisphere Hadley cell is nearly identical to that of the Oort data, and both circulation cells in the southern hemisphere are quite similar.

The data beyond 80° north or south do not appear to be reliable, and Oort does not include those regions for comparison.

Temperatures in the FGGE analysis (Fig. 3A) are quite representative of the climatological average. The only significant difference is that the equatorial stratosphere is slightly warmer.

Figure 3B shows the FGGE zonal mean specific humidity. The moisture field does not differ significantly from the climatological average.

The northward transport of momentum by the transient eddies (Fig. 5A) is very similar to that in Oort's climatology. Both the northern hemisphere maximum at about 30°N, 250 mb and the southern hemisphere minimum at about 40°S, 250 mb are quite similar to the corresponding figure for the Oort data (Fig. 6A). As with the wind fields, the data beyond 80° appears to be questionable.

The corresponding transport of momentum by stationary waves (Fig. 5B) is less representative of the climatological values. In the northern hemisphere, the maximum northward transport is similar to the climatological values, being located at about 30°N, 200 mb, but the amplitude is somewhat weak. Farther to the north, the (equatorward) transport is much stronger than the climatological

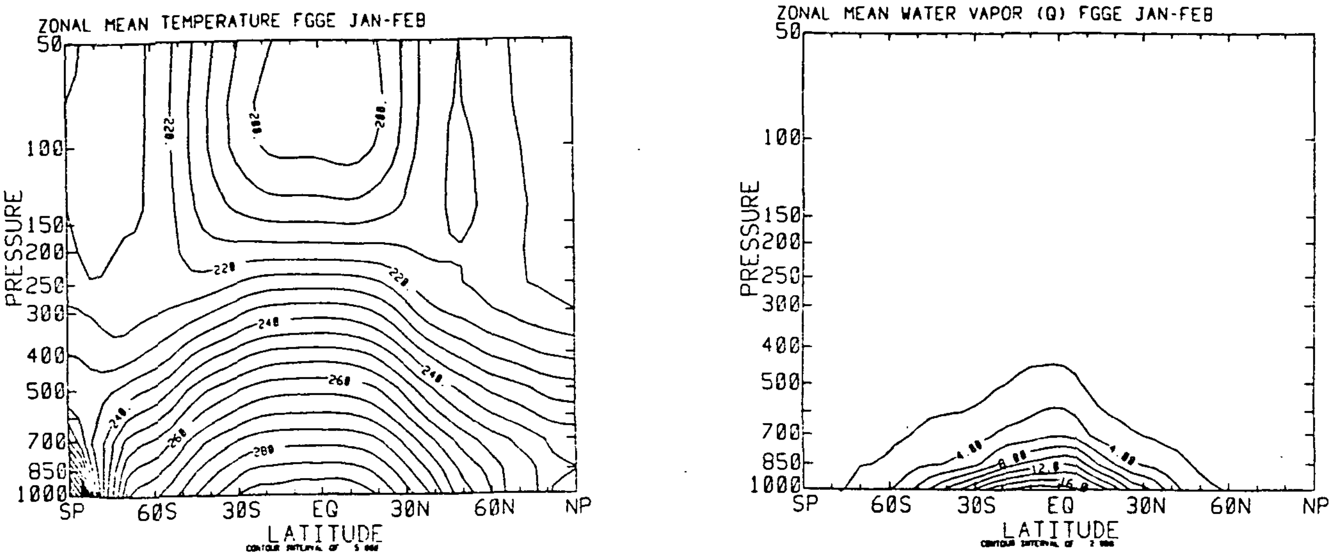

Fig. 3. Zonal mean temperature (^{o}K) and specific humidity for FGGE data

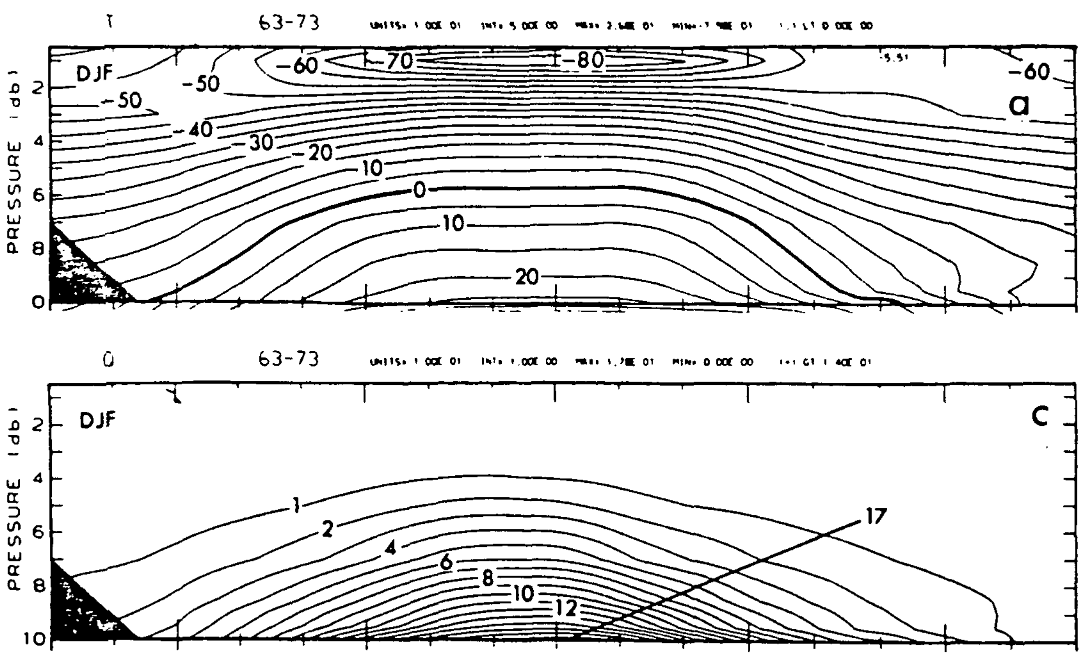

Fig. 4. Zonal mean temperature (^{o}C) and specific humidity for 11 years of winter data. (From Oort, 1983)

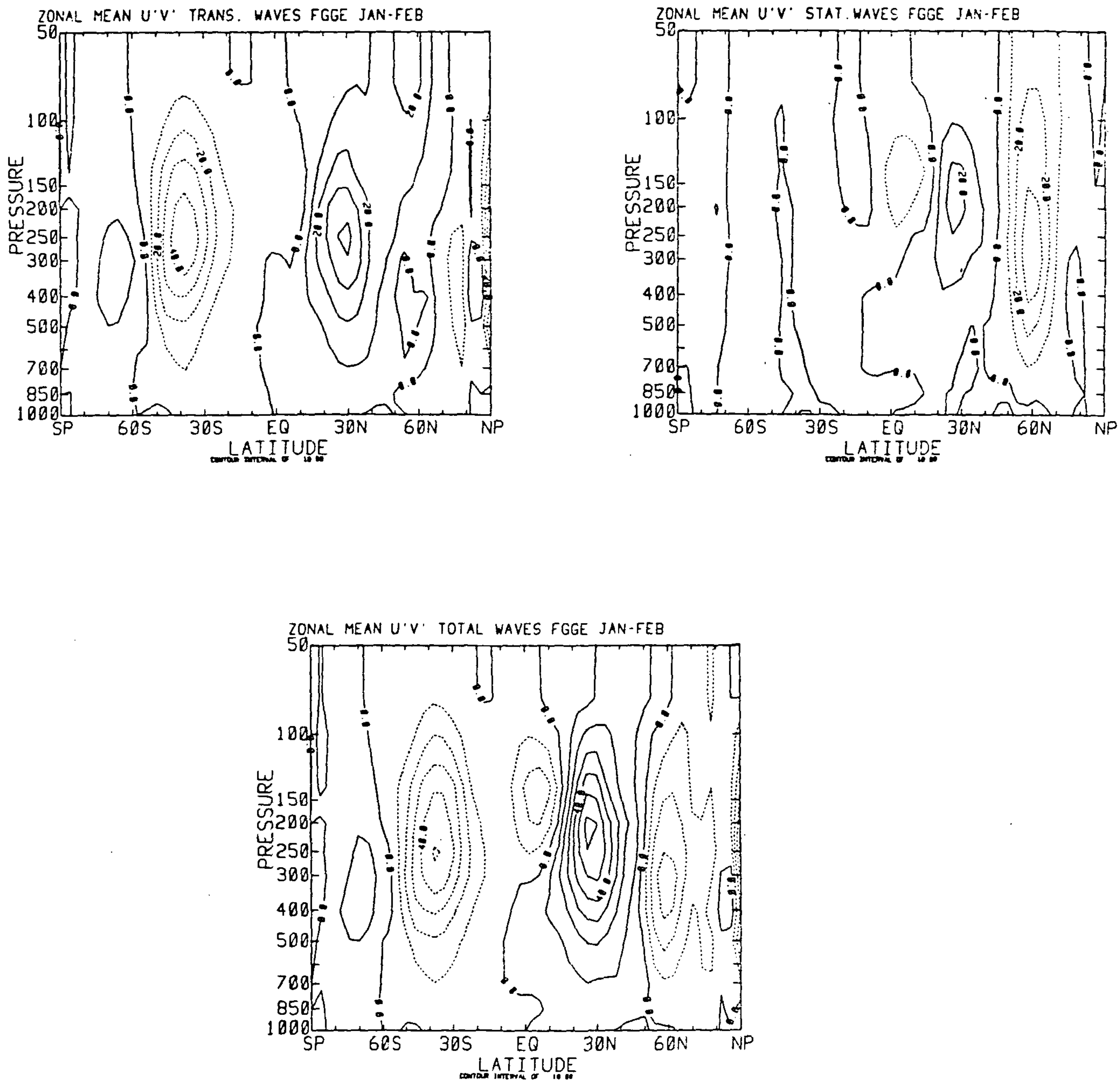

Fig. 5. Zonal mean northward transport of momentum by transient, stationary and total waves for FGGE data.

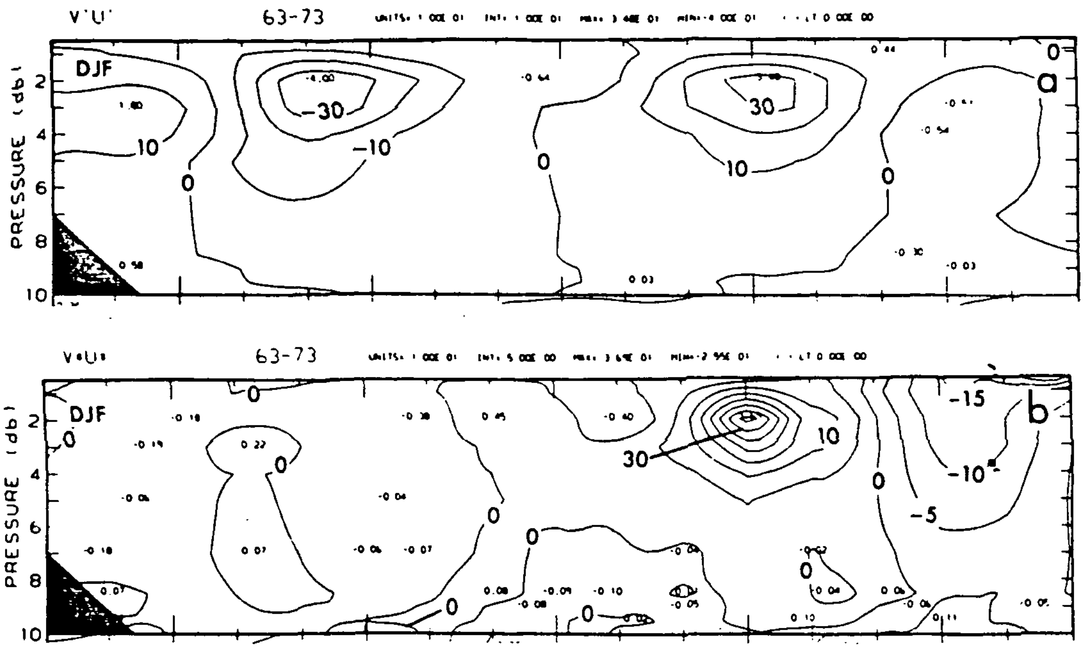

Fig. 6. Zonal mean northward transport of momentum by transient and stationary waves for 11 years of winter data. (From Oort, 1983)

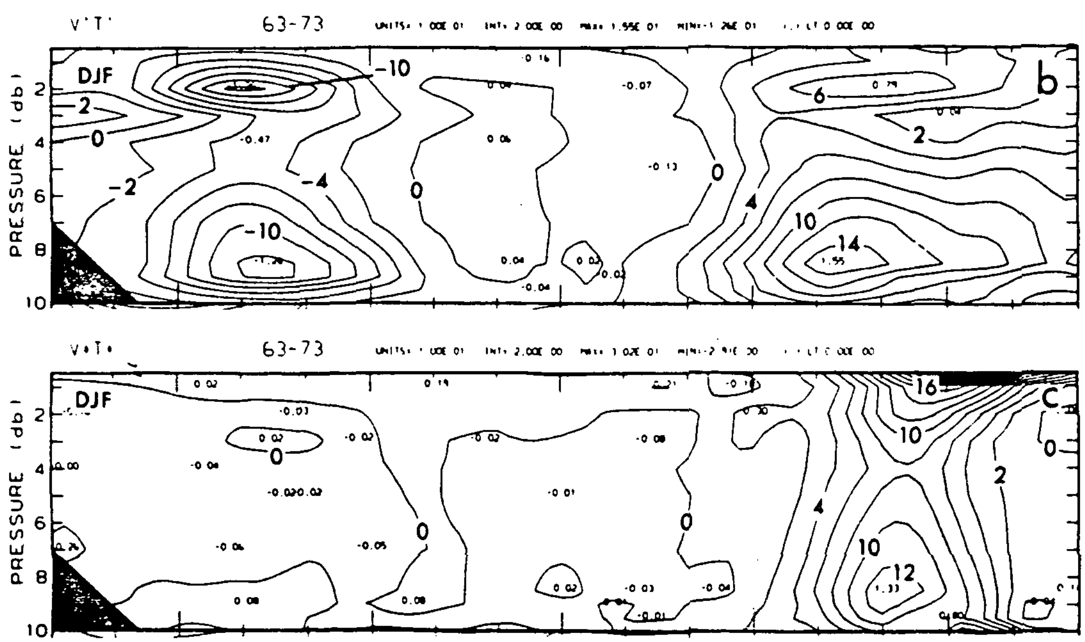

Fig. 7. Zonal mean northward transport of heat by transient and stationary waves for 11 years of winter data. (From Oort, 1983)

values and has its maximum at about 250 mb, whereas Oort's data shows the maximum equatorward transport to occur at 50 mb (the top level analyzed) north of 70°N.

The momentum transport by stationary waves is weak in the southern hemisphere, in both data sets, and the broad positive and negative regions match fairly well.

Overall, the meridional gradient of the momentum transport appears to be enhanced in the FGGE data. This will contribute to the wave driving of the mean wind through the divergence of the EP flux.

Figure 8A shows the northward heat transport by transient eddies. There are two unusual features in the FGGE data. The most obvious of these features is a maximum at about 10°N, 200 mb. This feature, which is absent in the Oort statistics, contributes a substantial vertical component of EP flux, (especially considering the low static stability in this region).

The maximum above 100 mb and north of 50°N is unusually large reflecting the very active stratosphere during Jan.-Feb. 1979. The rest of the regions are in good agreement with the Oort climatology.

Figure 8B shows the corresponding heat transport by stationary waves. The agreement with the Oort data is better. The entire field is weak except for a maximum between 40°N and 70°N. This feature is somewhat stronger above 100 mb in the FGGE data while it is weaker below 400 mb. Overall, the agreement is good.

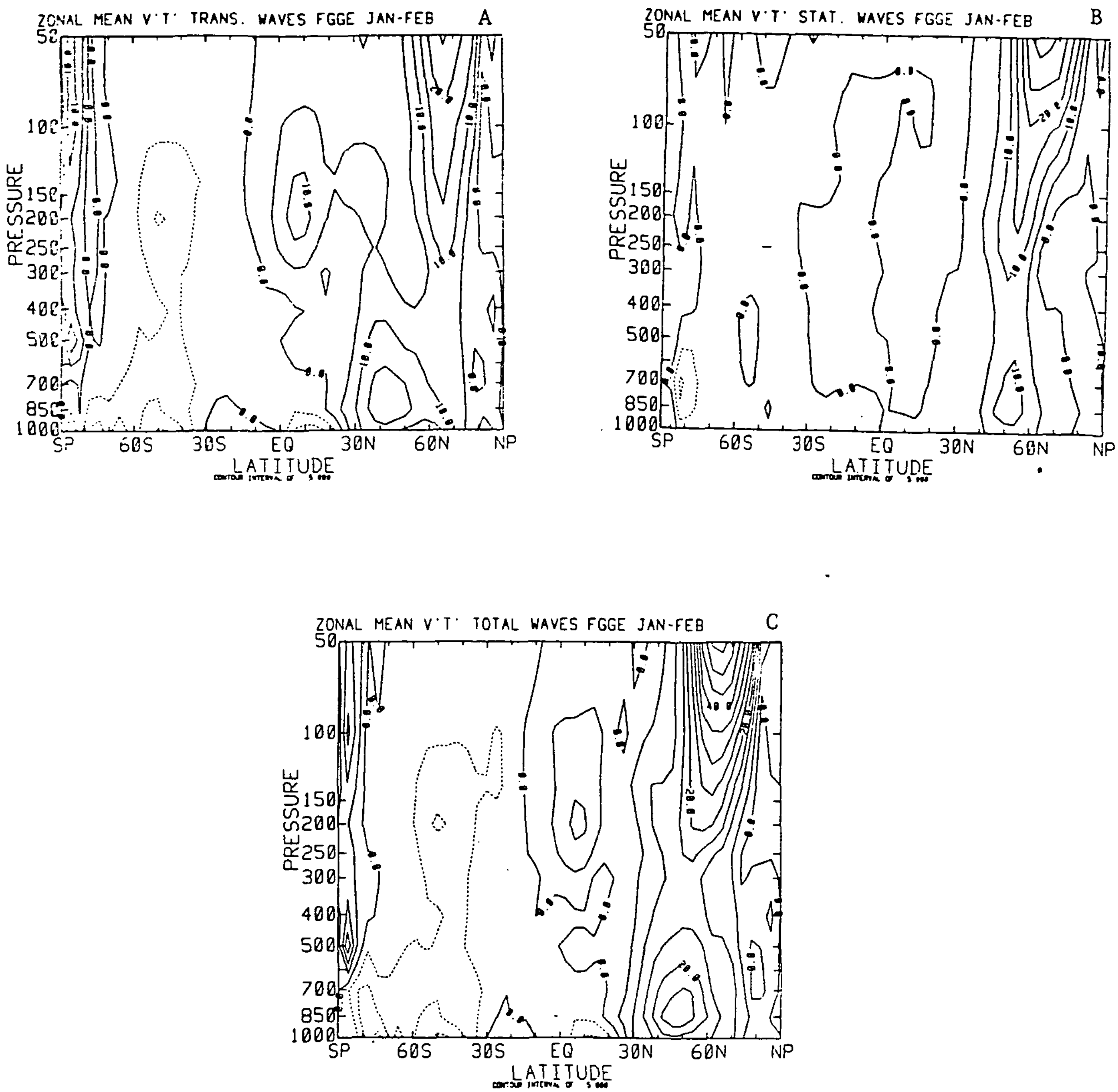

Fig. 8. Zonal mean northward transport of heat by transient, stationary, and total waves for FGGE data. The contour interval is 5 ms^{-1} ^oC

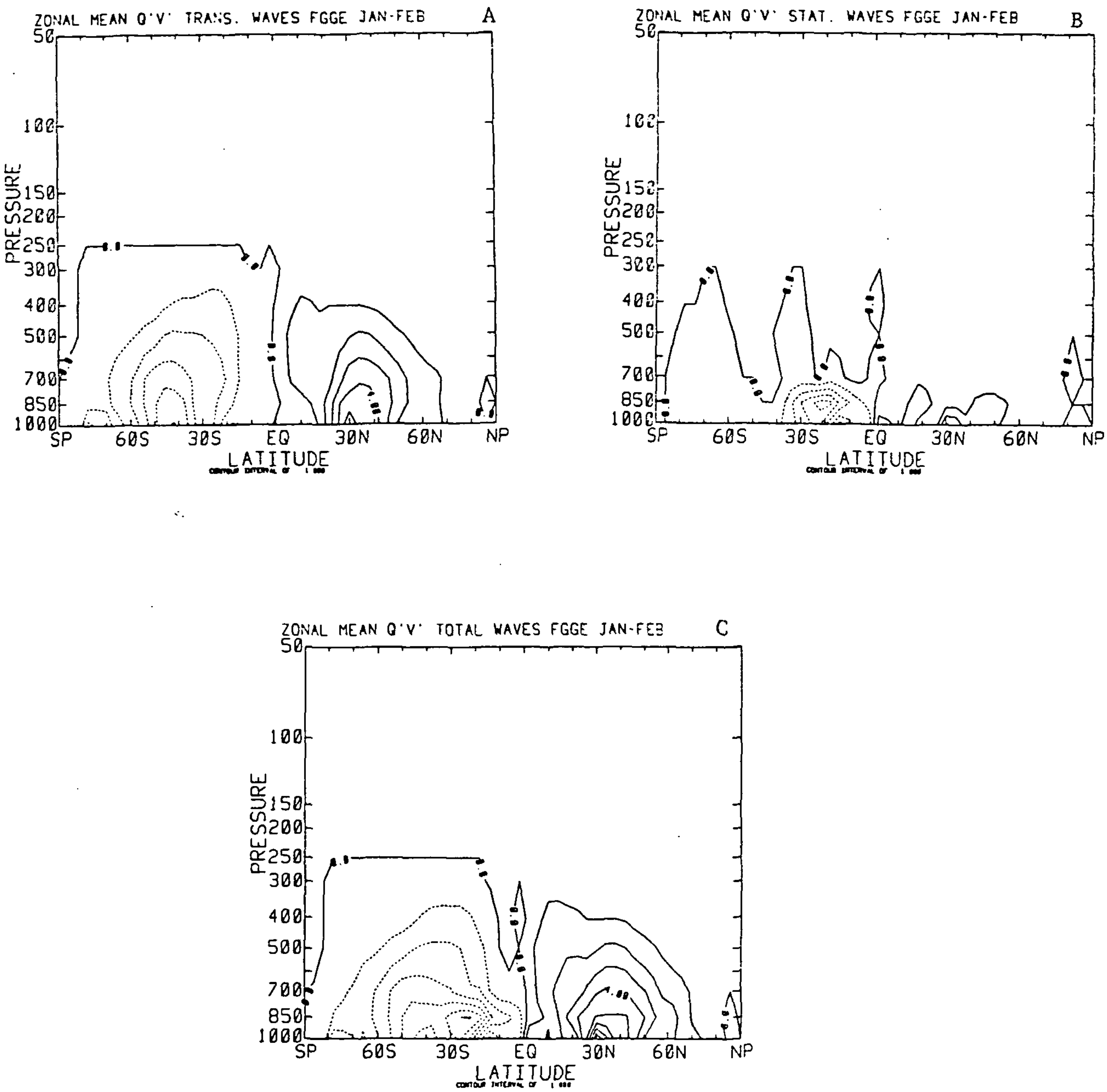

Fig. 9. Zonal mean northward transport of water vapor by transient, stationary and total waves for FGGE data. The contour interval is 1 gkg^{-1} ms^{-1}

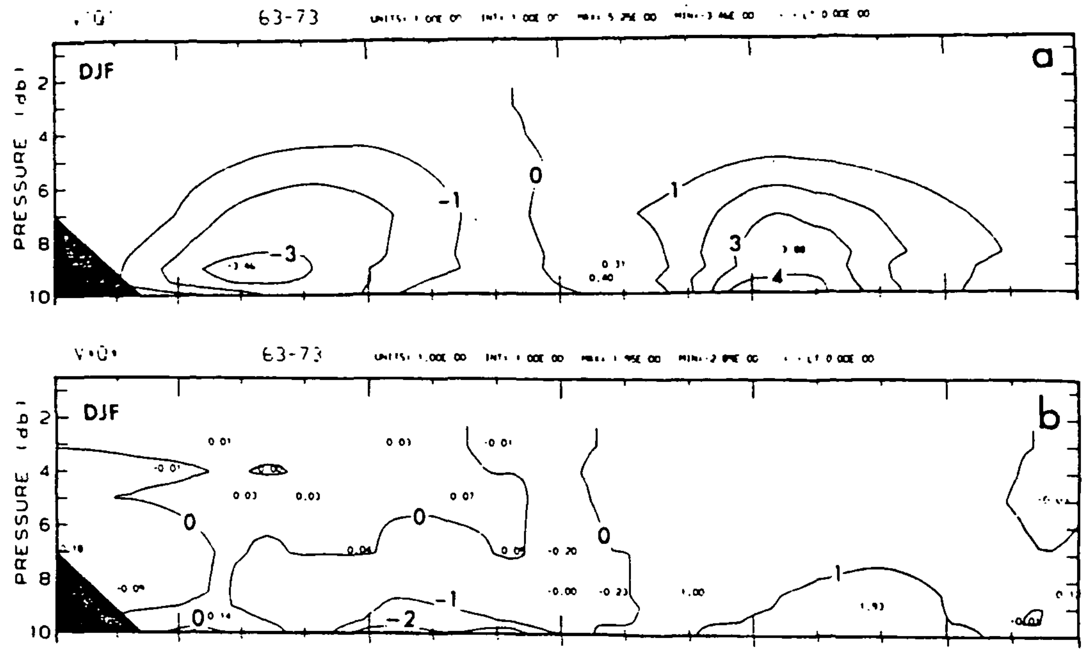

Fig. 10. Zonal mean northward transport of water vapor by transient and stationary waves for 11 years of winter data. (From Oort, 1983).

The transport of water vapor by transient eddies (Fig. 9A) does not differ significantly from the Oort data in the northern hemisphere. In the southern hemisphere, the transport is slightly stronger, with a maximum at 1000 mb. The maximum transport in the Oort data occurs at about 900 mb.

The corresponding figure for the standing waves (Fig. 9B) shows little transport in the northern hemisphere, while there is substantially enhanced transport in the southern hemisphere for the FGGE data. The maximum transport is almost twice that of the Oort data. However, Oort's maximum has broader latitudinal extent. Thus, the average transport in the 0° to 45°S belt is nearly the same in the two cases.

Figures 11A and 11B show the quasi-geostrophic potential vorticity and its northward gradient. The potential vorticity is given by (Hoskins, 1983):

$$(20) \quad \overline{q} = f + \overline{u}_y + f_0 \frac{\partial}{\partial p} (\theta'/d\Theta/dp)$$

where Θ represents the potential temperature for the standard atmosphere.

Figure 12A shows the streamfunction for the mean meridional circulation. This was calculated by integrating downward from 50 mb using the equation:

$$(21) \quad \overline{v} = - \frac{1}{2\pi r_0^2 \cos\phi} \frac{\partial \overline{\psi}}{\partial p}$$

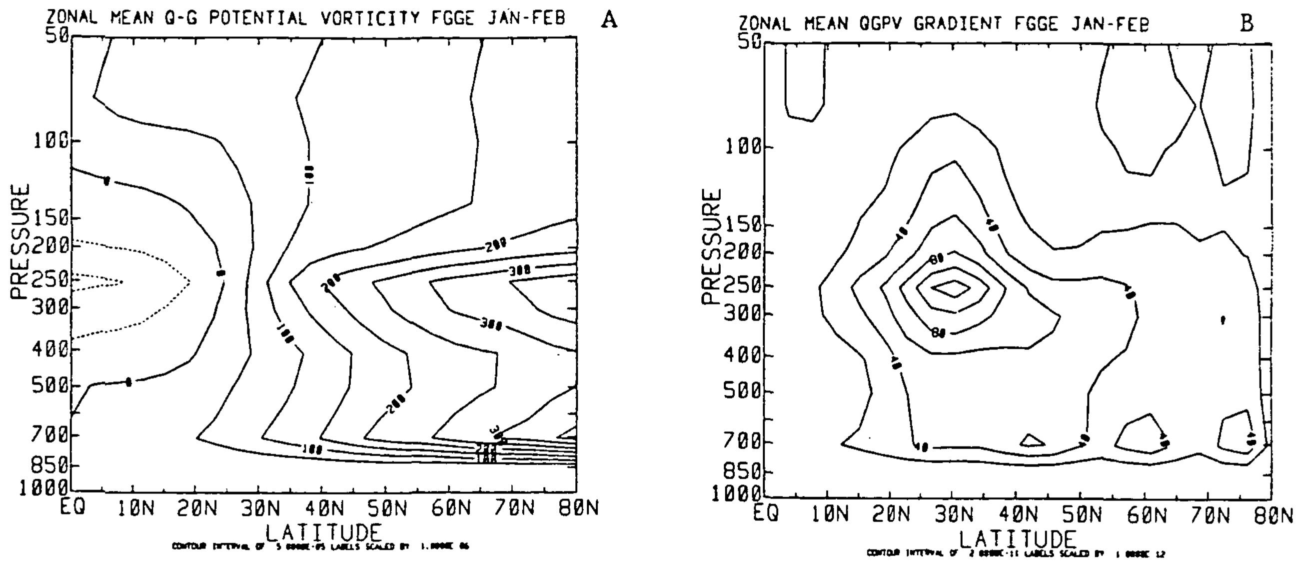

Fig. 11. Zonal mean quasi-geostrophic potential vorticity and potential vorticity gradient for FGGE data

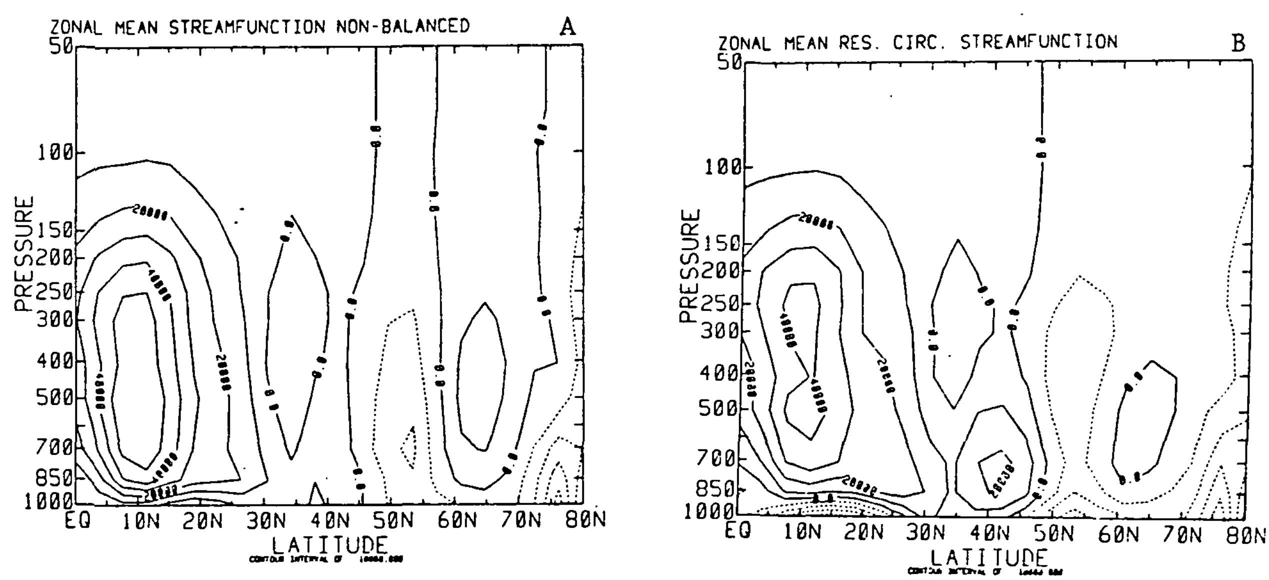

Fig. 12. Zonal mean streamfunction for the mean meridional circulation and streamfunction for the residual circulation for FGGE data

which is analogous to equation 14 which defines the mean residual circulation. The pressure coordinate form was chosen for ease of computation. The Hadley cell is quite reasonable, but the Ferrel cell circulation is not as clean. This is probably due to the short observing period and inaccuracies in the original data. However this deviation is small.

The residual circulation, which arises as a response to the eddy-induced torque on the zonal mean flow, is shown in figure 12B. This was also calculated using equation (21) by integrating downward from 50 mb, but using v* instead of v. A comparison with Figure 6A of Edmon <u>et al</u>. shows that circulation for the FGGE SOP-1 period differed substantially from that of Edmon <u>et al</u>. north of 30°N. The pattern is dominated by smaller-scale circulations, rather than the one large circulation as calculated by Edmon <u>et al</u>.

Figures 13-17 are the equivalent of figures 1, 3, 5, 8, and 9 but for the northern hemisphere only. They are shown in this form to facilitate comparison with the EP flux diagrams.

b) The EP diagrams, Figures 18a and b, show the transient eddy EP fluxes for the FGGE and Oort data, respectively. The EP flux patterns are very similar, except for the region near 200 mb south of 15°N. As can be seen in Figure 16a, there is a large heat flux. This region has a fairly low static stability, so the resulting vertical flux component is quite large.

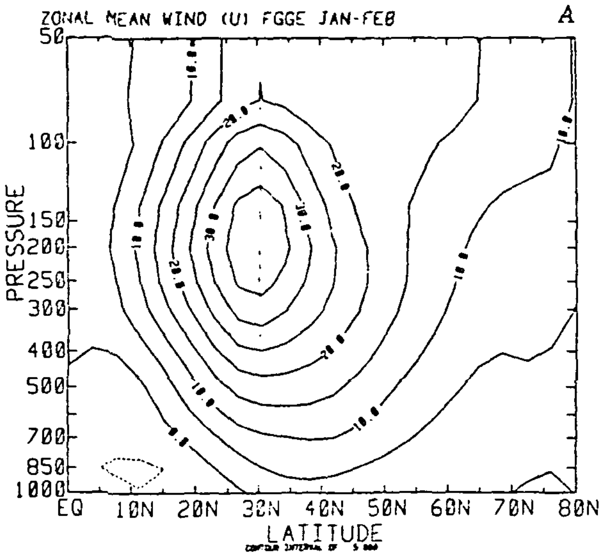

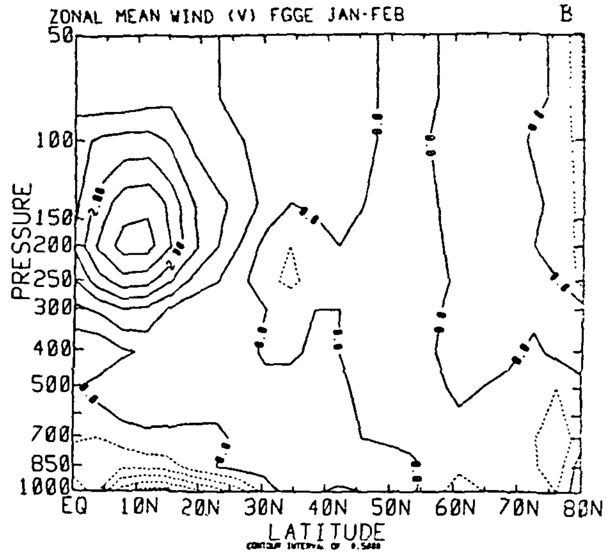

Fig. 13. Zonal mean zonal wind and meridional wind components for FGGE data.

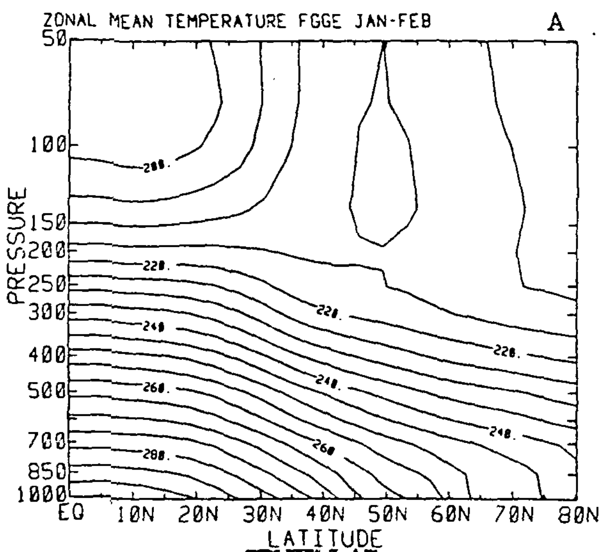

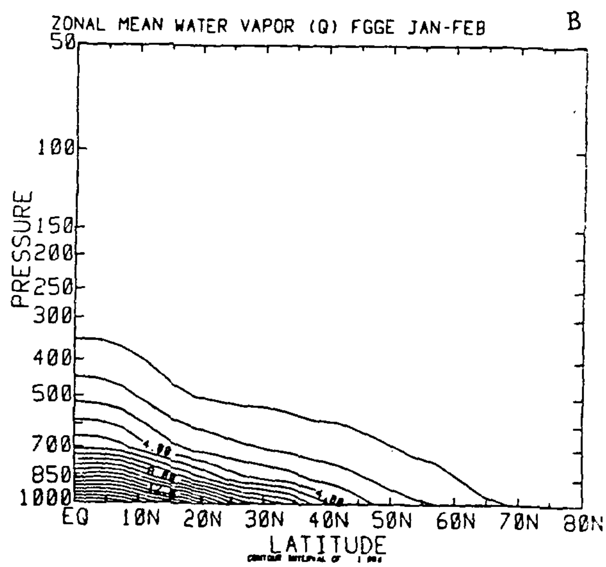

Fig. 14. Zonal mean temperature and specific humidity for FGGE data.

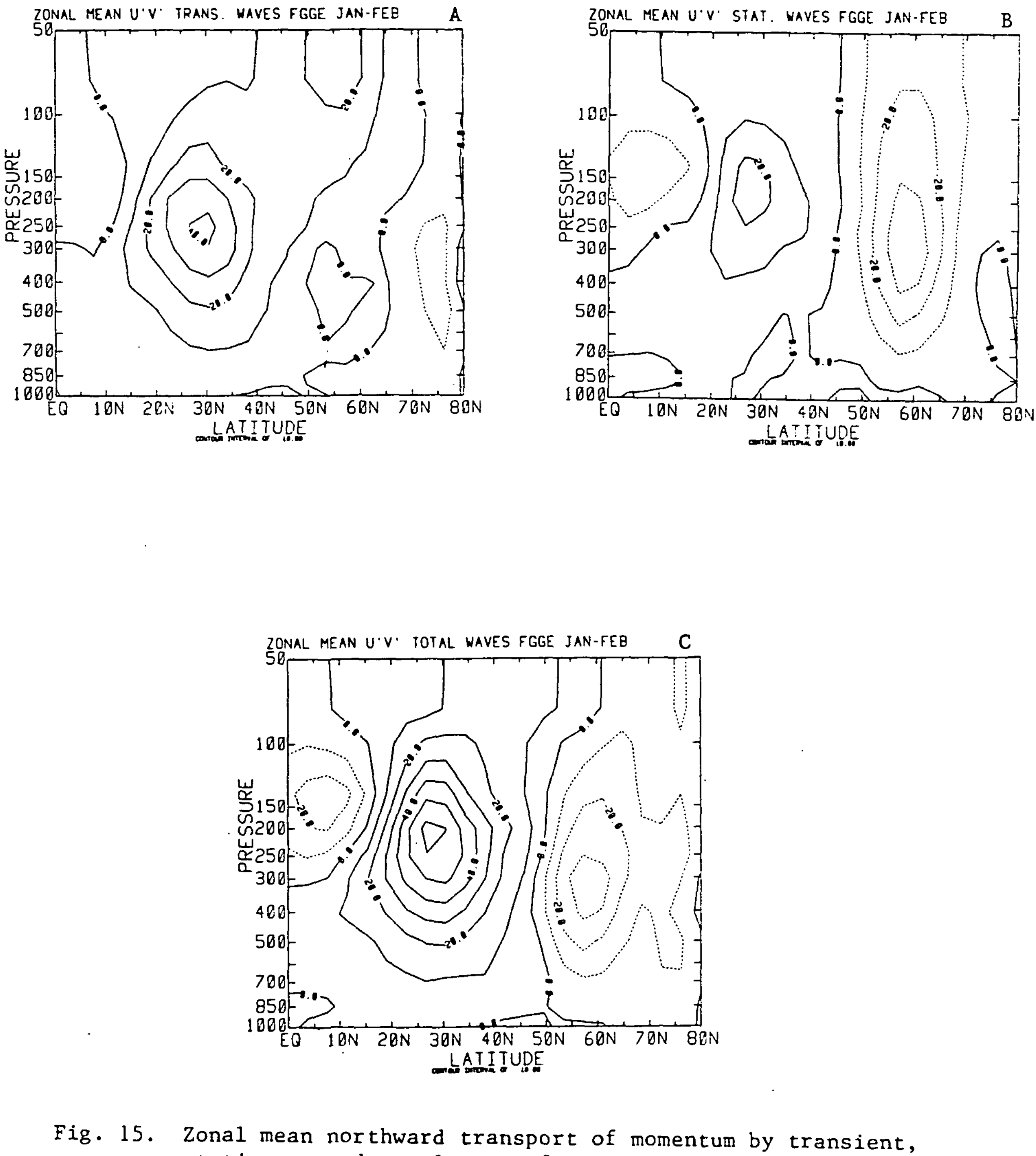

Fig. 15. Zonal mean northward transport of momentum by transient, stationary and total waves for FGGE data.

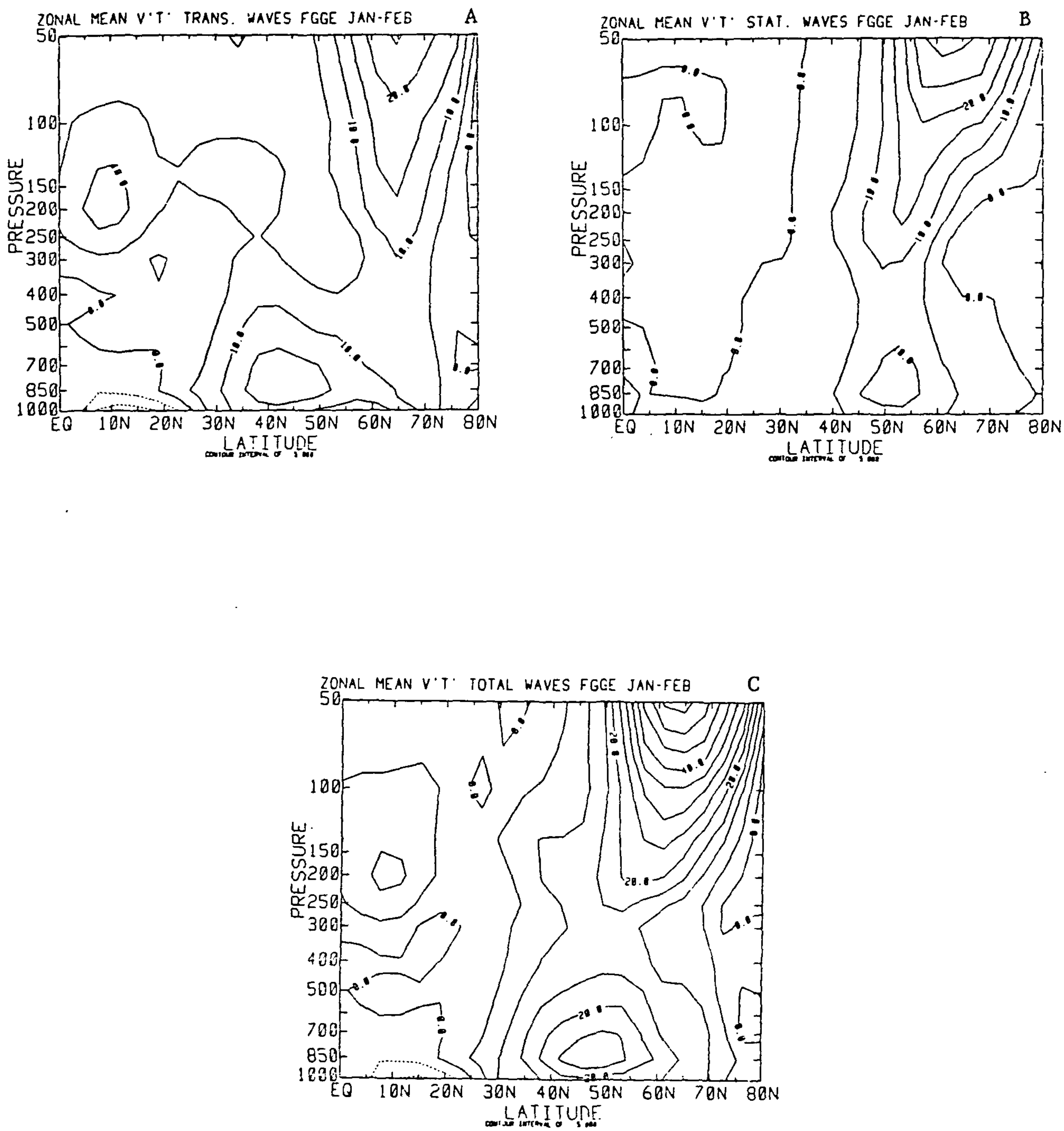

Fig. 16. Zonal mean northward transport of heat by transient, stationary and total waves for FGGE data.

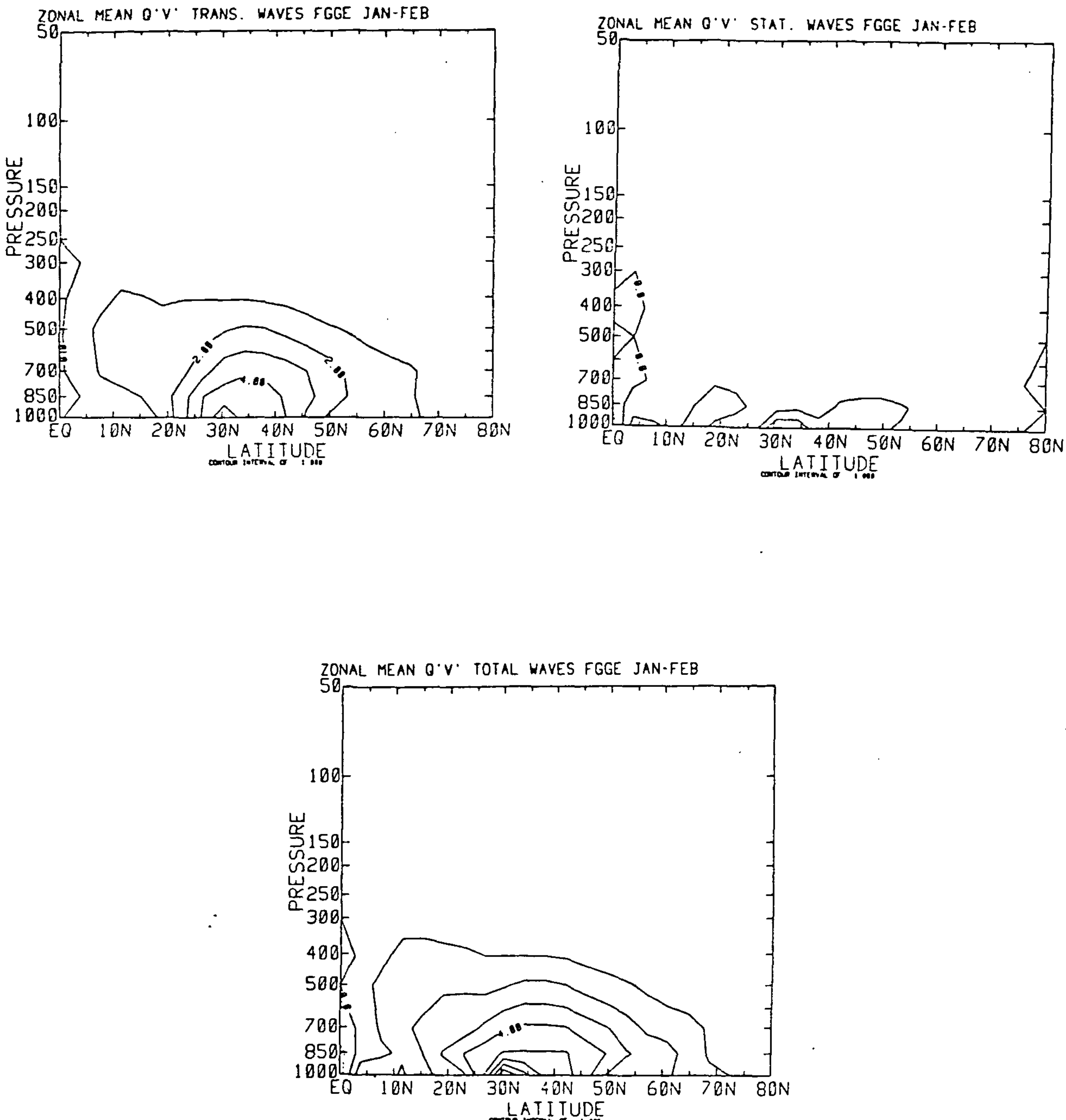

Fig. 17. Zonal mean northward transport of water vapor by transient, stationary and total waves for FGGE data. The contour interval is 1 gkg^{-1} ms^{-1}

The overall regions of divergence and convergence match fairly well. The maximum near 70°N at 50 mb is the result of the unusually large heat flux in that region. Near 10°N and 250 mb there is substantial divergence, while there is convergence in the Oort statistics. This is the result of the anomalous heat flux maximum in this region.

The EP flux patterns for stationary waves (Figs. 18c and 18d) are very similar. There is an unusually large equatorward momentum flux near 200 mb and 10°N and the southward momentum fluxes north of 50°N are quite large.

The most unusual feature is the convergent region near 70°N and 400 mb. This feature is the result of the unusually large momentum flux and flux gradient in this region (Fig. 13b). The equatorward transport of momentum north of 50°N is probably the result mainly of wave number 2, which has an amplitude maximum near 60°N and westward phase tilt with increasing latitude.

Figures 19a and 19b show EP fluxes for the total waves. These figures have greater similarity than either the transient or stationary wave diagrams. This suggests that the partitioning between stationary and transient waves for the relatively short SOP-1 may have resulted in too little of the divergence/convergence being assigned to the stationary waves north of 50°N.

Strong heat fluxes in the tropics are still evident, and the associated EP flux divergence indicates that an unusual eddy source occurred there.

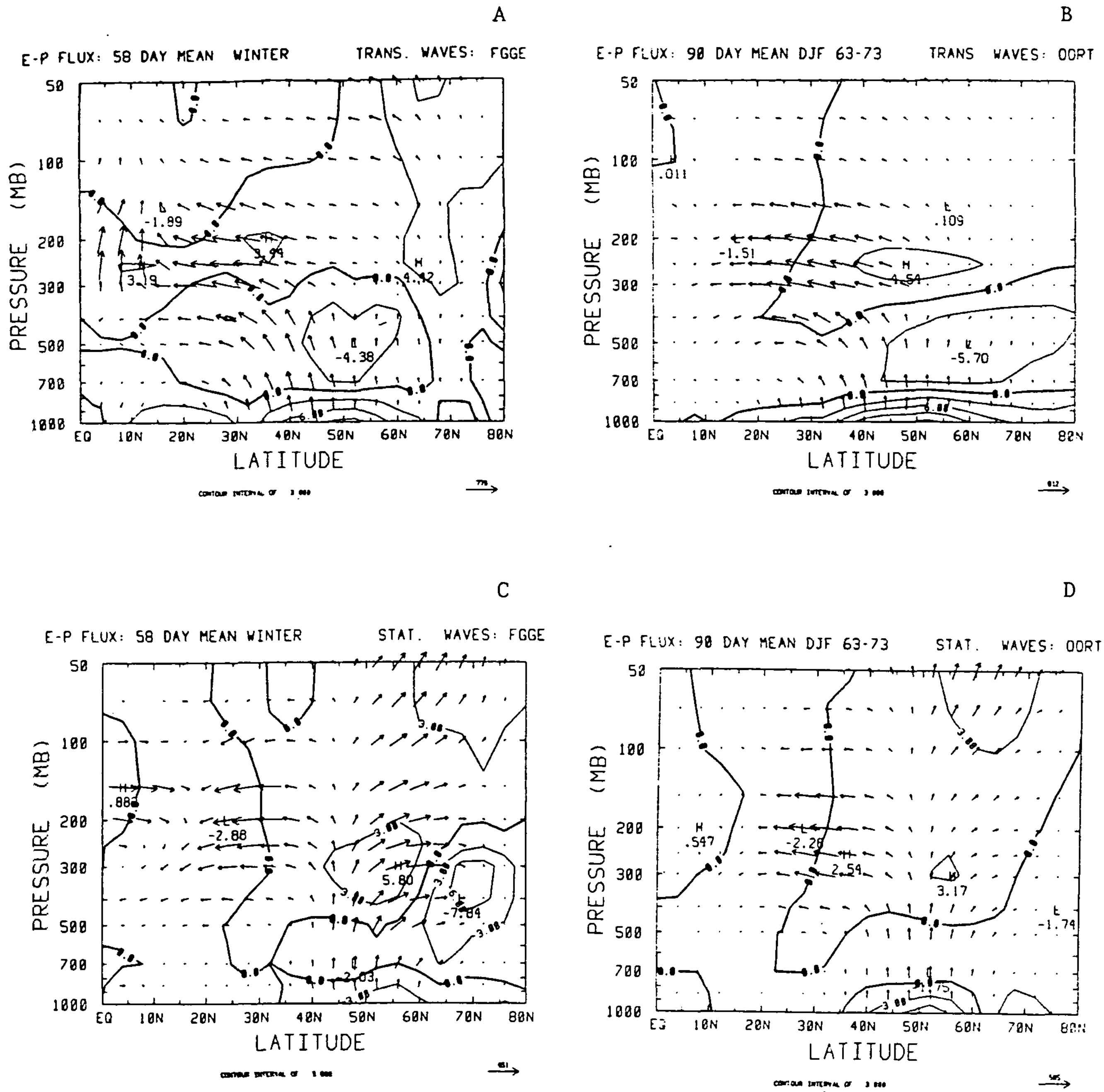

Fig. 18. Eliassen-Palm flux by transient and stationary waves for FGGE and Oort (1983) data. The contour interval is 3 ms^{-1} day^{-1}

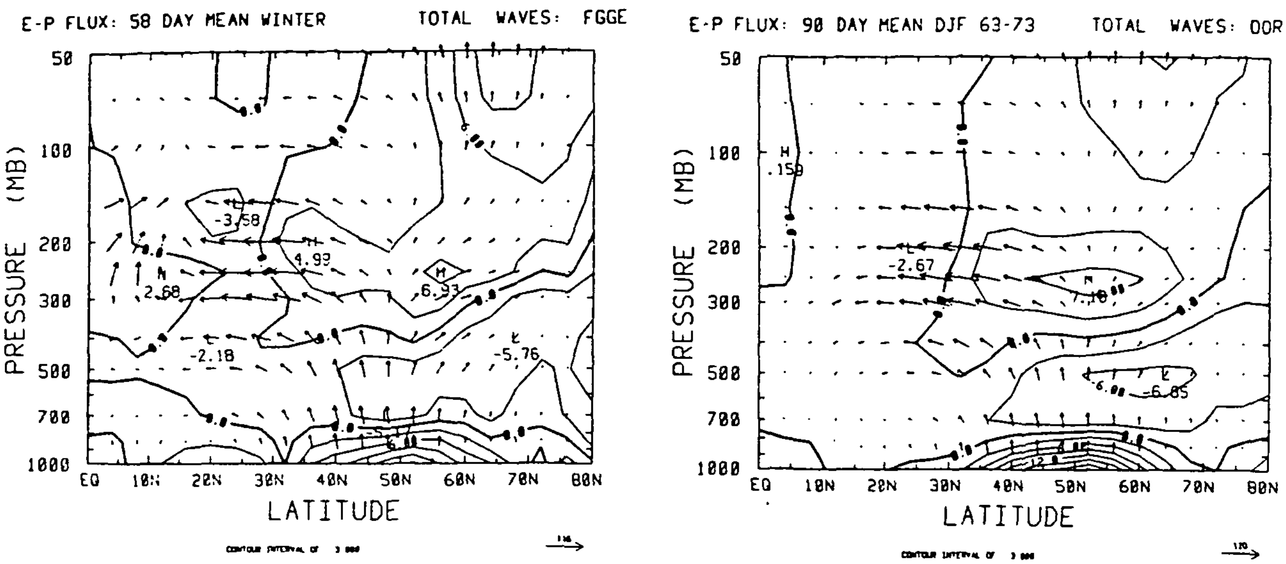

Fig. 19. Eliassen-Palm diagrams for total waves for FGGE and Oort (1983) data. The contour interval is 3 ms^{-1} day^{-1}

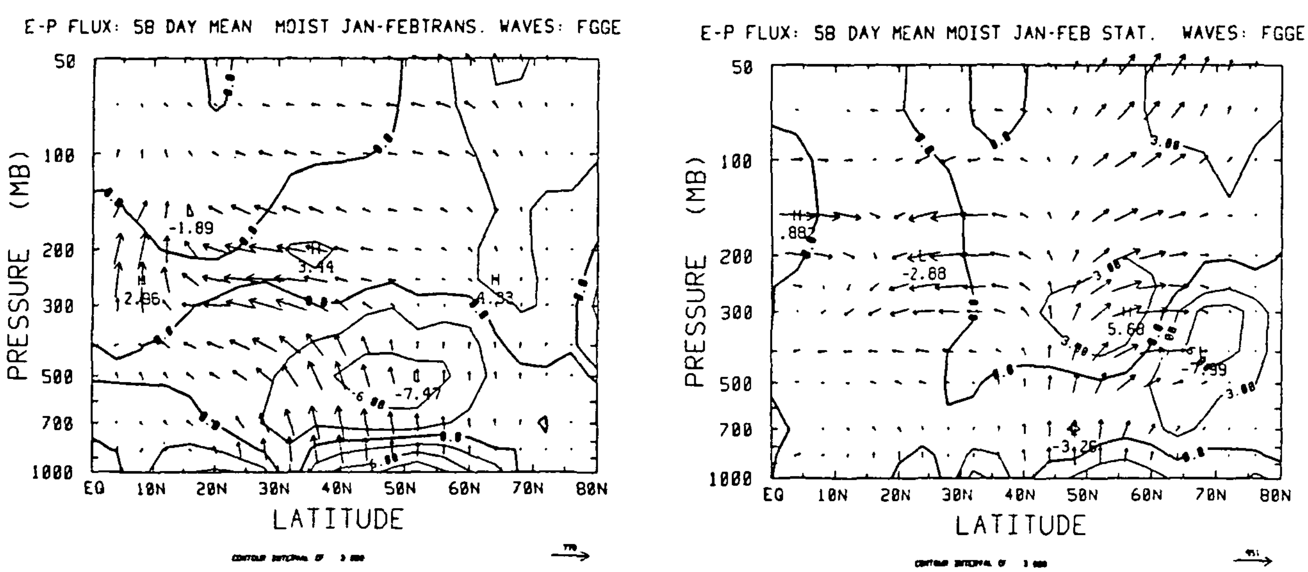

Fig. 20. Eliassen-Palm diagrams for transient and stationary waves using FGGE data including eddy moisture flux. The contour interval is 3 ms^{-1} day^{-1}

The EP diagrams 20a, 20b and 21 include eddy moisture flux

$$(p_0/p)^{R/c_p} (L/c_p)\, \overline{v'q'}$$

as discussed in Section 2. These "moist" EP flux diagrams correspond to Figures 18a, 18c and 19a.

In all the "moist" diagrams, the pattern of EP flux is nearly the same as those without the moisture term, only being increased in the mid-latitude lower troposphere. The EP flux divergence tends to be amplified below 400 mb in the mid-latitudes and the lower tropospheric divergence tends to be slightly farther north.

The main effect is that the eddy moisture flux tends to amplify the existing pattern below 400 mb in mid-latitudes.

Overall, the EP cross sections using the FGGE data are remarkably similar to those calculated using the Oort data. The main differences are easily traced back to isolated unusual features in either the heat or momentum fluxes during the FGGE winter. Some unusual features in the transient or stationary wave diagrams may be due to using a 58-day average with the FGGE data and a 90-day average with the Oort data. The close similarity between the EP fluxes in these two data sets indicates that the FGGE SOP-1 period was close to the climatological average in most respects.

Figures 22, 23a and 23b show FGGE EP fluxes for the southern hemisphere summer. There is a substantial area of divergence near

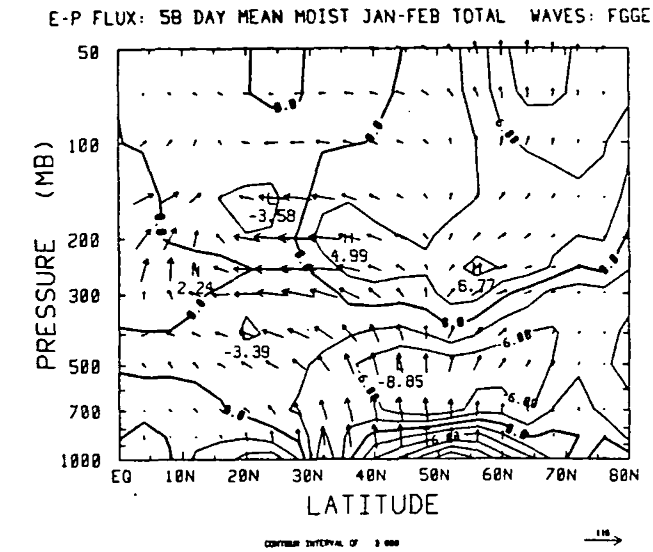

Fig. 21. Eliassen-Palm diagram for total waves using FGGE data including eddy moisture flux

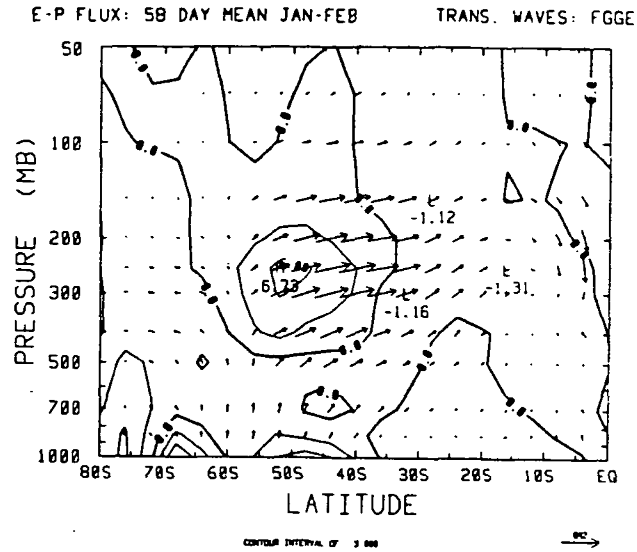

Fig. 22. Eliassen-Palm diagram for transient waves, southern hemisphere, using FGGE data

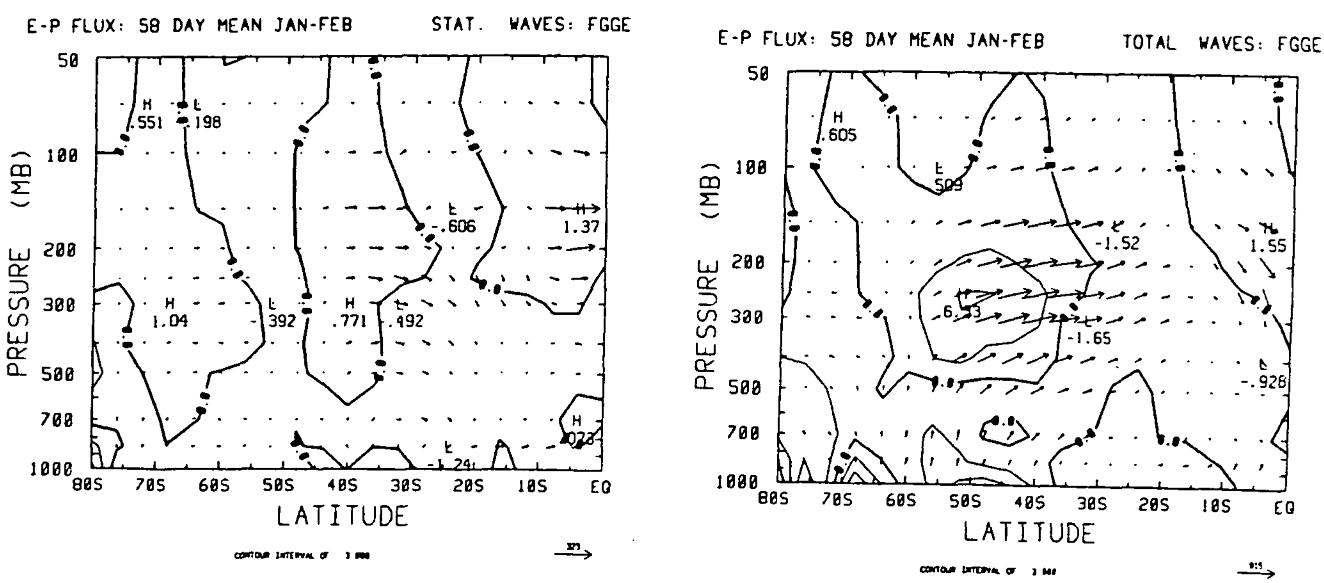

Fig. 23. Eliassen-Palm diagram for stationary and total waves, southern hemisphere, using FGGE data.

50°S and 300 mb in the transient wave diagram, with strong poleward momentum transports to the north.

The pattern for the stationary waves is extremely weak, and consequently, the pattern for the total waves looks almost exactly like that for the transient waves.

Figures 24, 25, and 26 show 5-day mean EP fluxes for the transient waves. The patterns of divergence are quite noisy, but the arrows seem to be consistent. There were two unusual events which occurred at at high latitudes. During days 1-10, there are no major features north of 60° above 500 mb. But during the next 15 days a large region of divergence seemed to propagate down from above 50 mb while simultaneously developing at about 400 mb by days 20-30, this region seems to have retreated back into the stratosphere above 100 mb. This event corresponds to a stratospheric sudden warming.

The second event was even stronger, and was related to the wave number 2 sudden stratospheric warming discussed in Palmer (1982). Note that during days 30-40 there was a large area of convergence between 300 and 500 mb north of 50°N. By days 41-45 a region of divergence had replaced this convergent region, and it extended up to 50 mb. During the next 5 days a very strong region of divergence had developed over the entire region above 500 mb north of 60°. This divergence, averaged over five days, indicates a forcing of the zonal wind of more than 25 ms^{-1} day^{-1} at both 300 mb and 50 mb. During days 40-45, the usual poleward momentum flux was reversed.

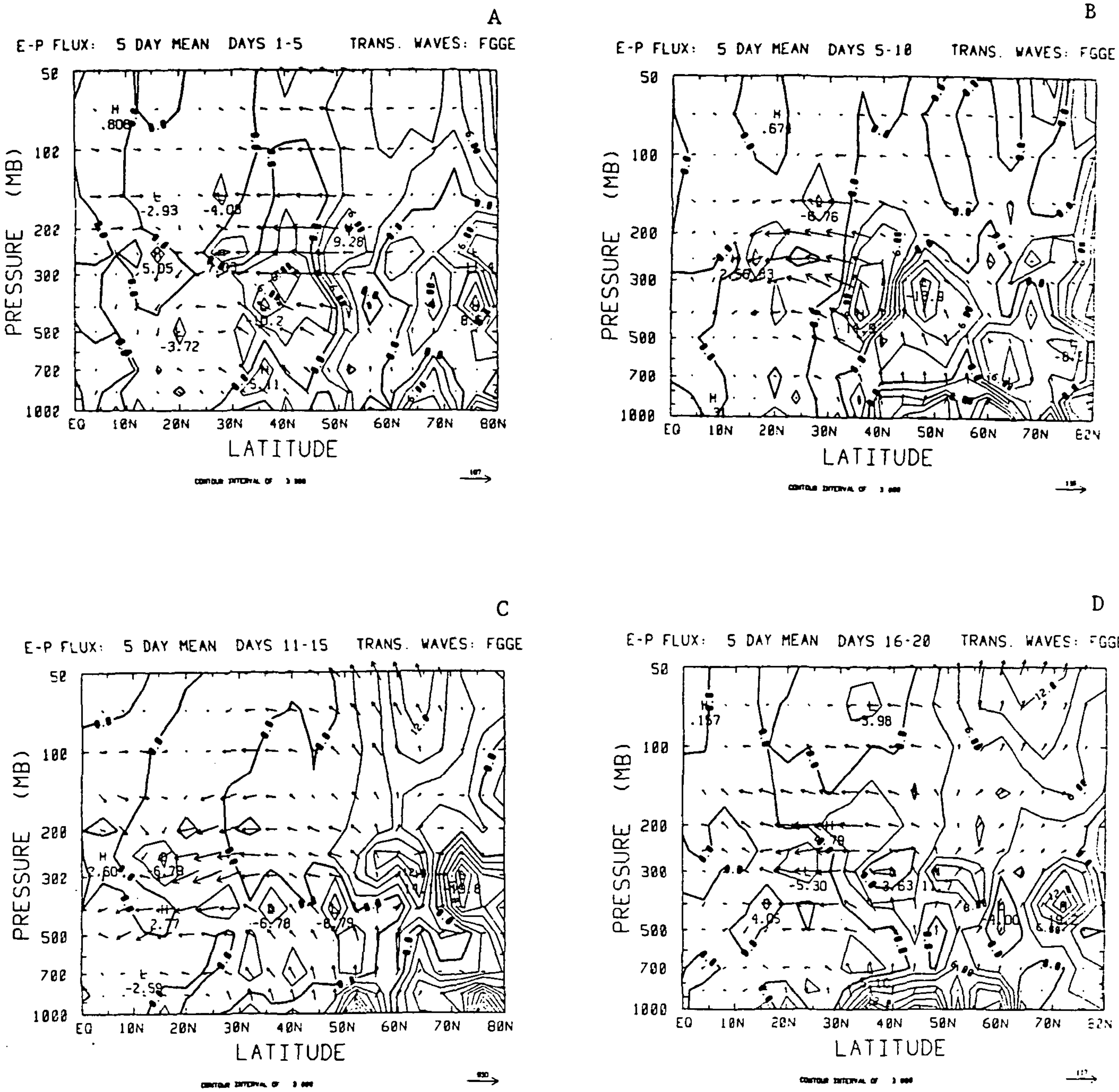

Fig. 24. 5-day mean Eliassen-Palm diagrams for transient waves using FGGE data

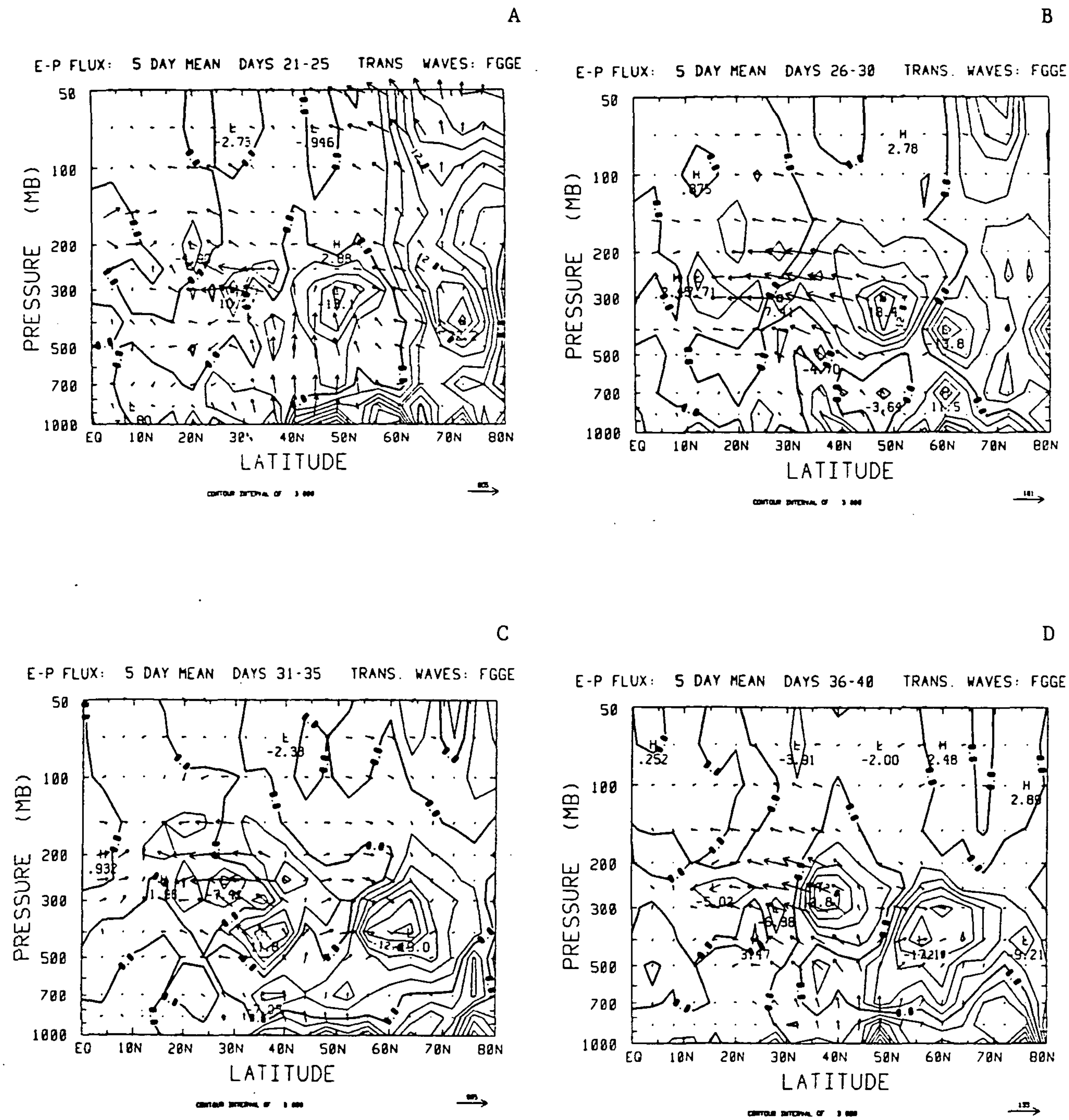

Fig. 25. 5-day mean Eliassen-Palm diagrams for transient waves using FGGE data

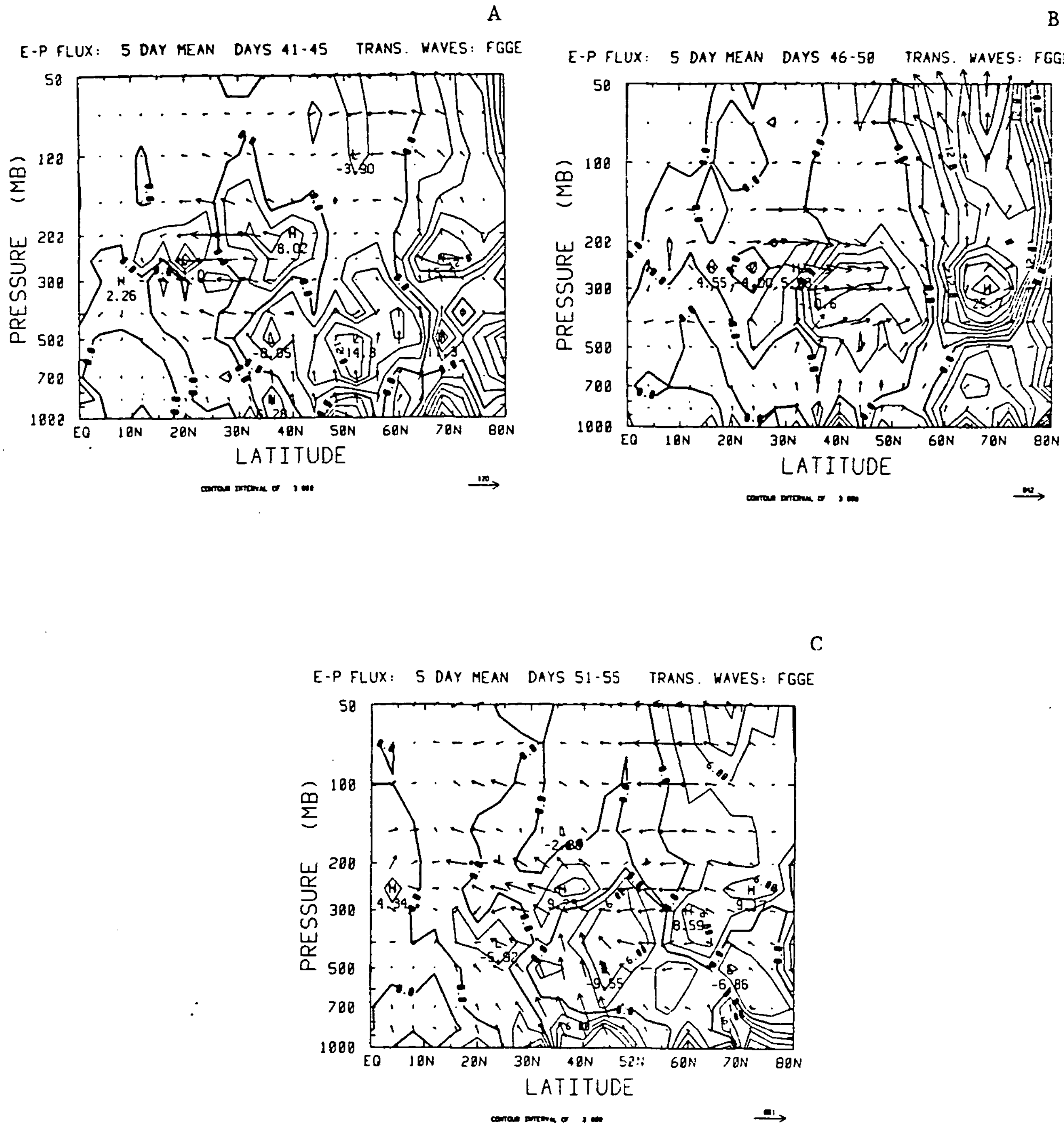

Fig. 26. 5-day Eliassen-Palm diagrams for transient waves using FGGE data

It is only during this one five-day period that this happened. This equatorward momentum flux is probably associated with the divergence near 70°N at 300 mb. It is not clear from these 5-day means whether the divergence propagated up from the upper troposphere or developed simultaneously in the stratosphere and troposphere.

To try to determine the source of the divergence, a series of 1-day means to days 44-51 (Figs. 27, 28) was made. These 1-day means are very noisy. During days 44, 45, and 46, the divergence at about 300 mb, 65°N developed rapidly. This was a source of wave activity which propagated vertically into the stratosphere. The momentum fluxes near 300 mb were not well organized during this period.

On days 47 and 48, the equatorward momentum fluxes developed near 40°N and 300 mb. The region of divergence above 200 mb deepened considerably. By day 49 the entire area north of 60° above 500 mb was a source of wave activity which propagated upward and equatorward. Throughout the mid-latitudes, strong equatorward momentum fluxes were convergent near 55°N.

This strong momentum flux pattern disappeared by day 50, and the only strong divergence was above 150 mb. By day 51, there was nothing unusual in the pattern.

During this event, a strong source of wave activity developed near 300 mb and near 50 mb. Wave activity tended to propagate upward from the 300 mb region and through the source near 50 mb. The rever-

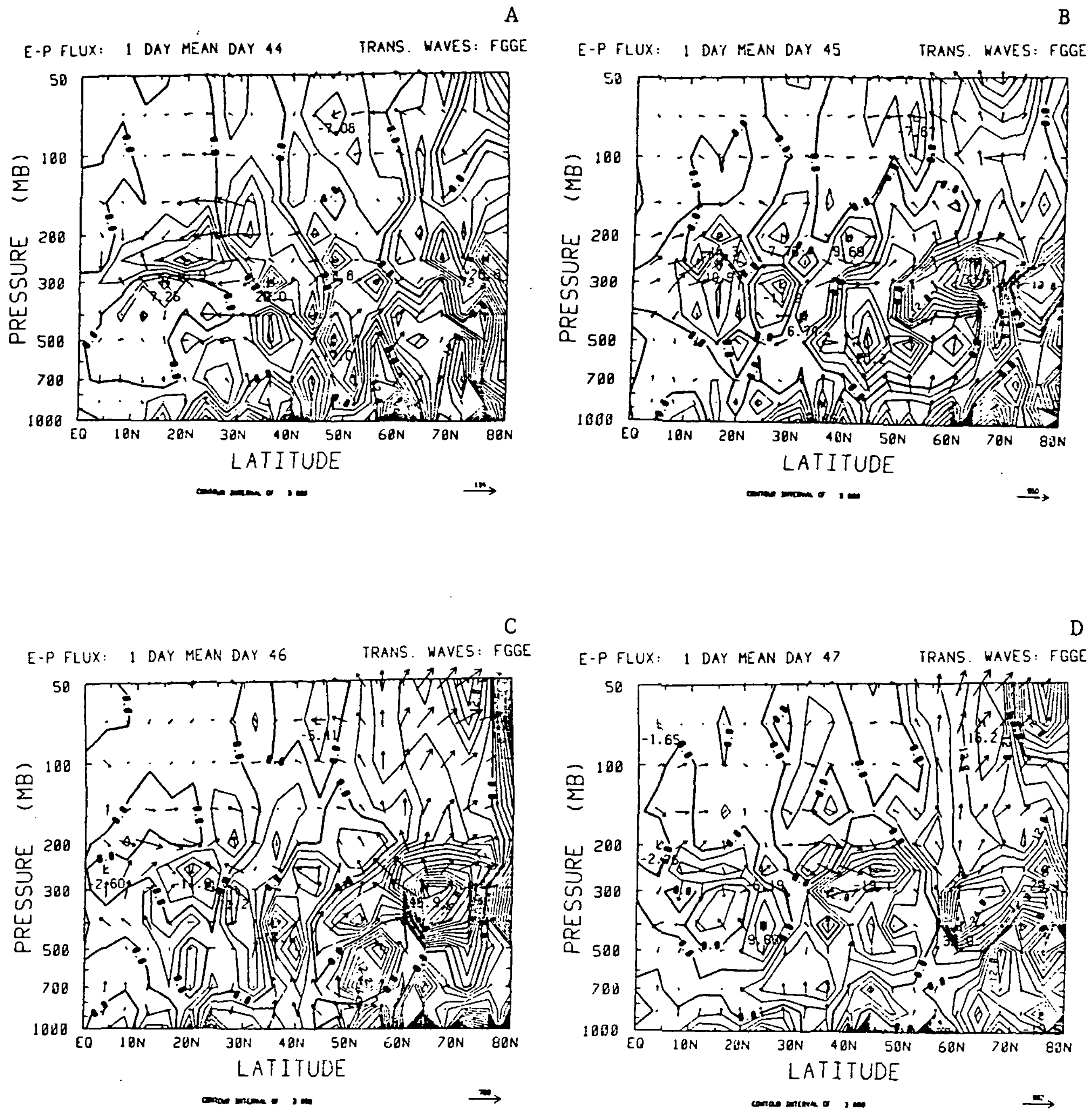

Fig. 27. 1-day mean Eliassen-Palm diagrams for transient waves days 44-47 using FGGE data

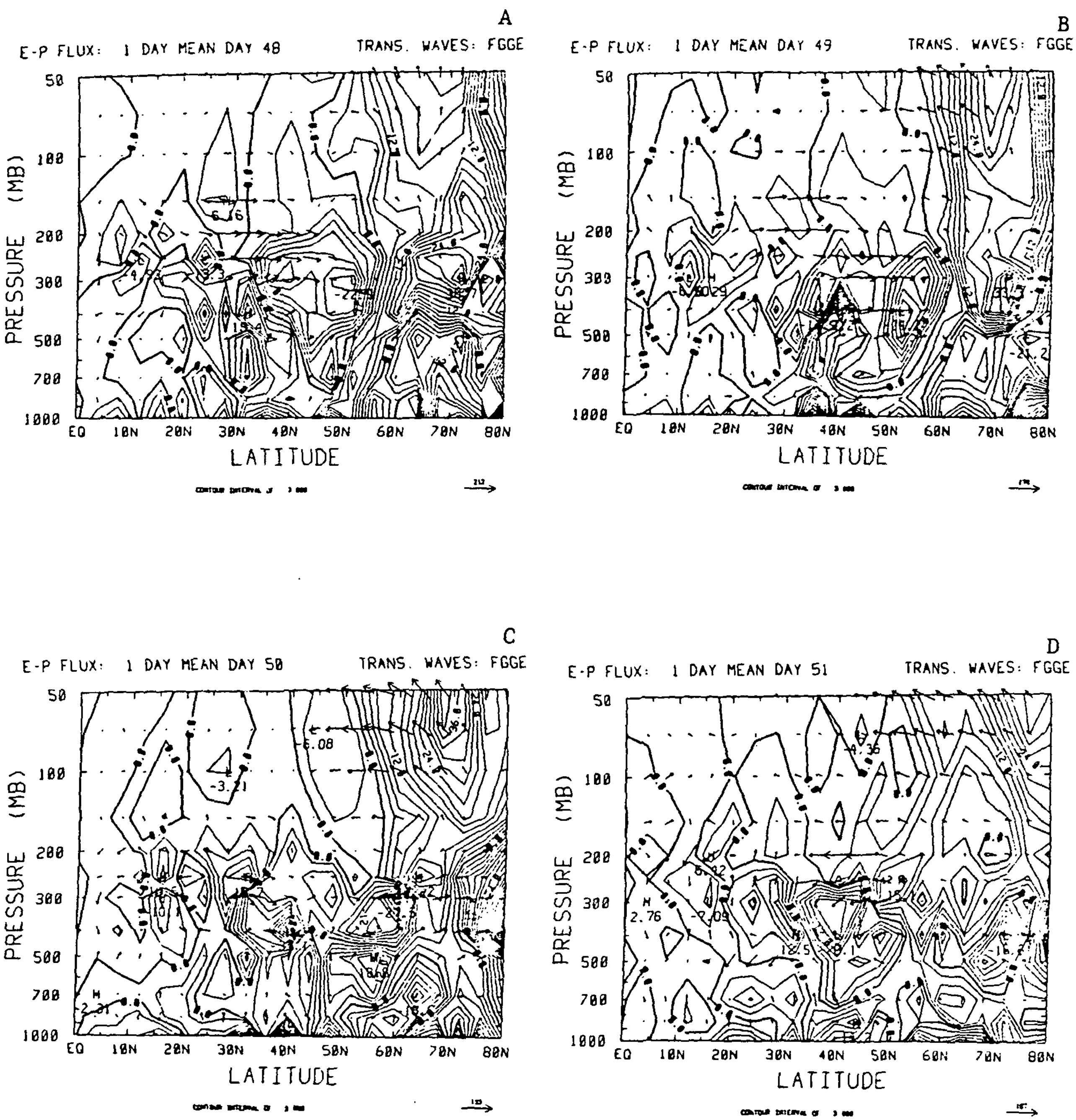

Fig. 28. 1-day mean Eliassen-Palm diagrams for transient waves, days 48-51, using FGGE data

sal of the momentum fluxes in the mid-latitudes seems to be associated with the event.

c. Cross spectral analysis

Time series, similar to those of Hartmann et al. (1984), of daily values of $\partial u/\partial t$ and the wave driving by the eddies were calculated for two regions in the meridional plane. The compensating residual circulation $f\bar{v}^*$ was also calculated. In order to determine the effects of oscillations of different frequencies, cross spectral analysis was performed.

Figures 29 and 30 are for the region 36°N to 60° and 200 to 500 mb. Figure 29 is for the wave driving and the mean wind changes alone, while Figure 30 includes the $f\bar{v}^*$ term.

The day-to-day relationship between $\partial u/\partial t$ and the wave driving was not strong, with a correlation coefficient of .339. The magnitude of the wave driving was typically much greater than $\partial u/\partial t$. When the $f\bar{v}^*$ term is included, the correlation coefficient was only .056. One would expect the relationship to be better with $f\bar{v}^*$ included.

Figure 29c indicates that most of the cross covariance comes from oscillations with periods of more than a week. The graph of the coherence, Fig. 28d, is erratic. Since the correlation coefficient is only .056 for Figure 30 and the coherence squared is very low, clearly the relationship is weak.

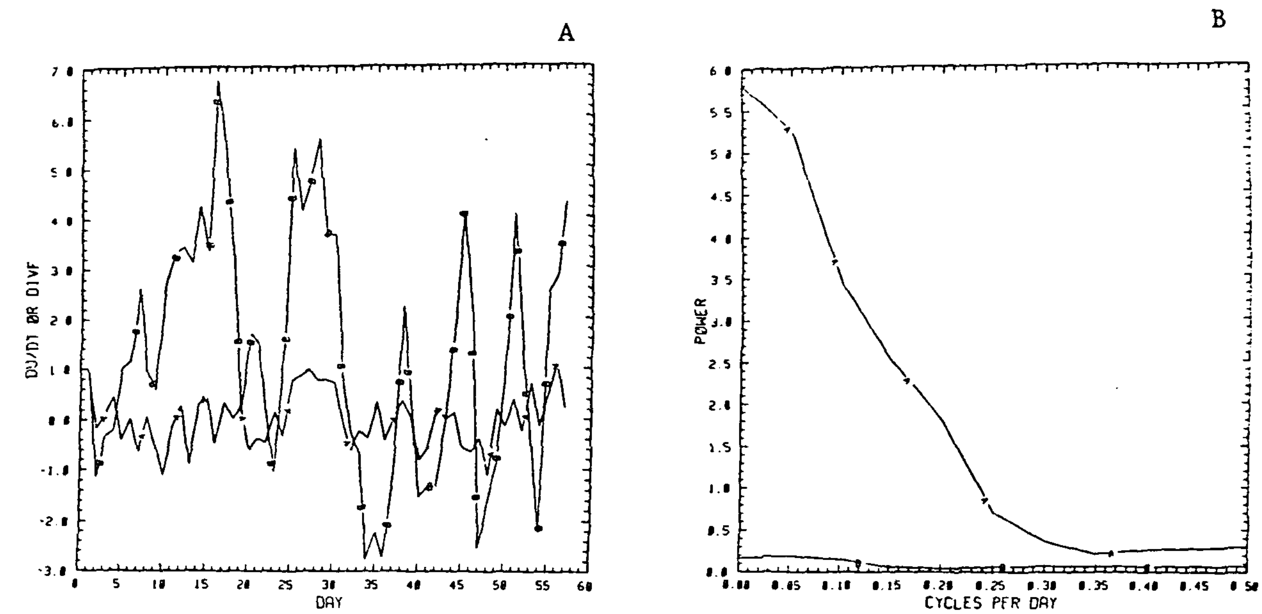

Line A represents $\partial u/\partial t$

Line B represents $\partial u/\partial t$

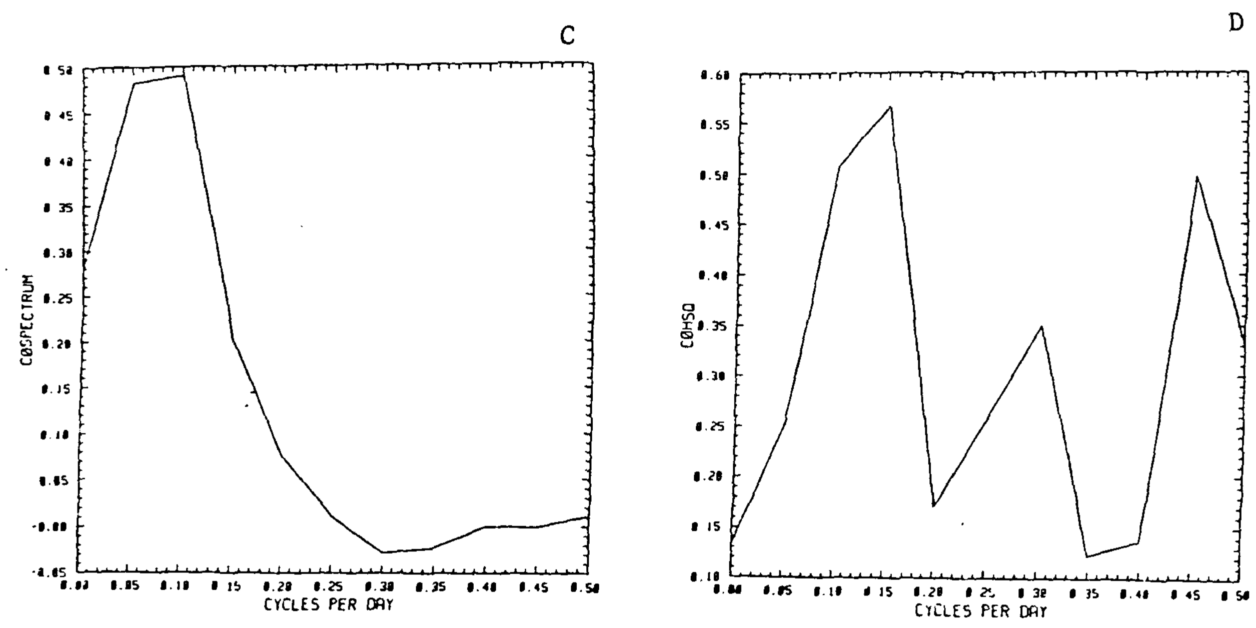

Fig. 29. Cross spectrum analysis for 36°N to 60°N, 200 mb to 500 mb, for FGGE data. $\partial u/\partial t$ vs wave forcing.

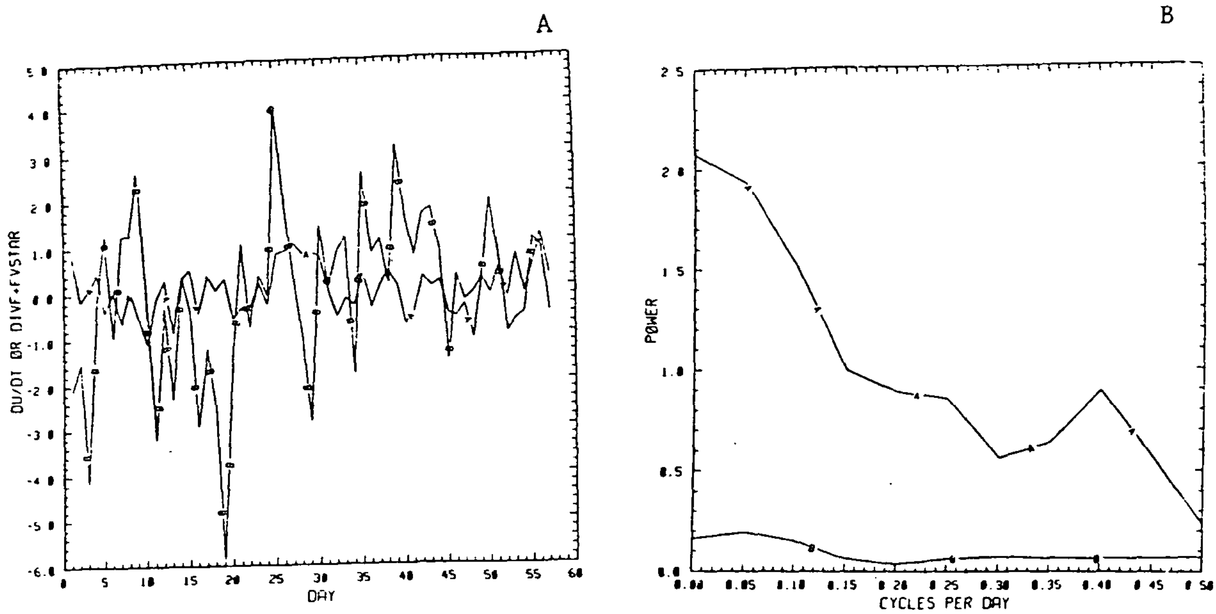

Line A represents $\partial u/\partial t$

Line B represents $\partial u/\partial t$

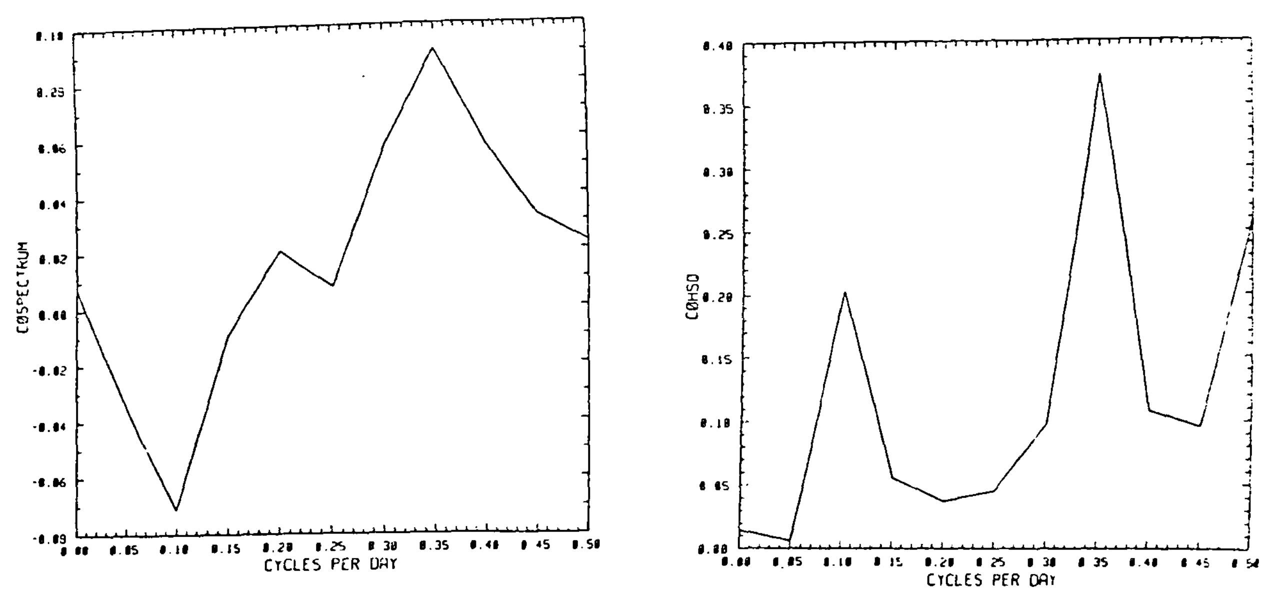

Fig. 30. Cross spectrum analysis for 36°N to 60°N, 200 mb to 500 mb, for FGGE data, including $f\bar{v}^*$ term.

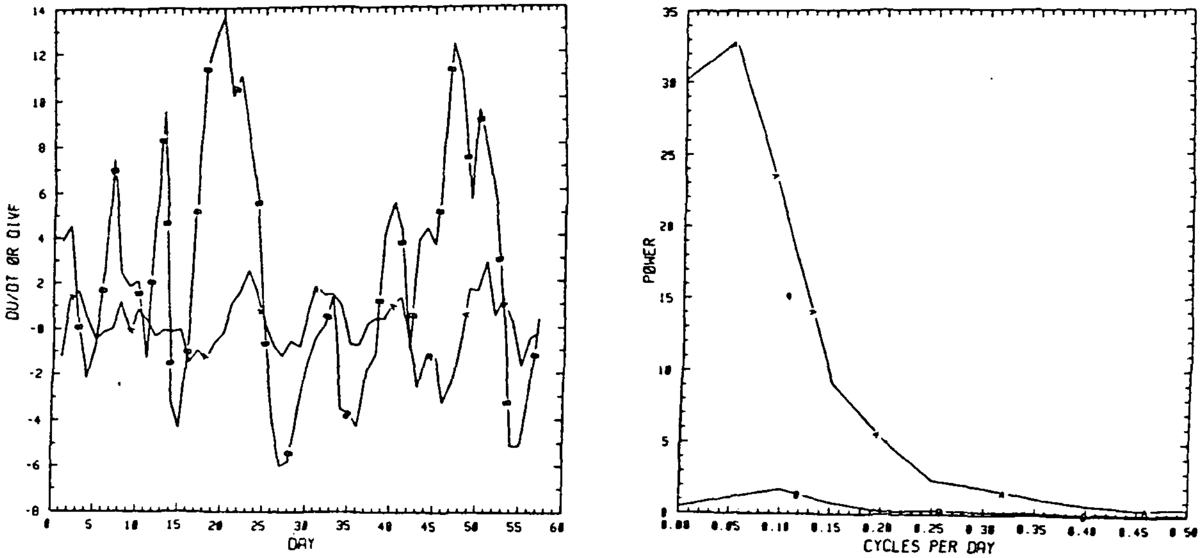

Line A represents $\partial u/\partial t$ Line B represents $\partial u/\partial t$

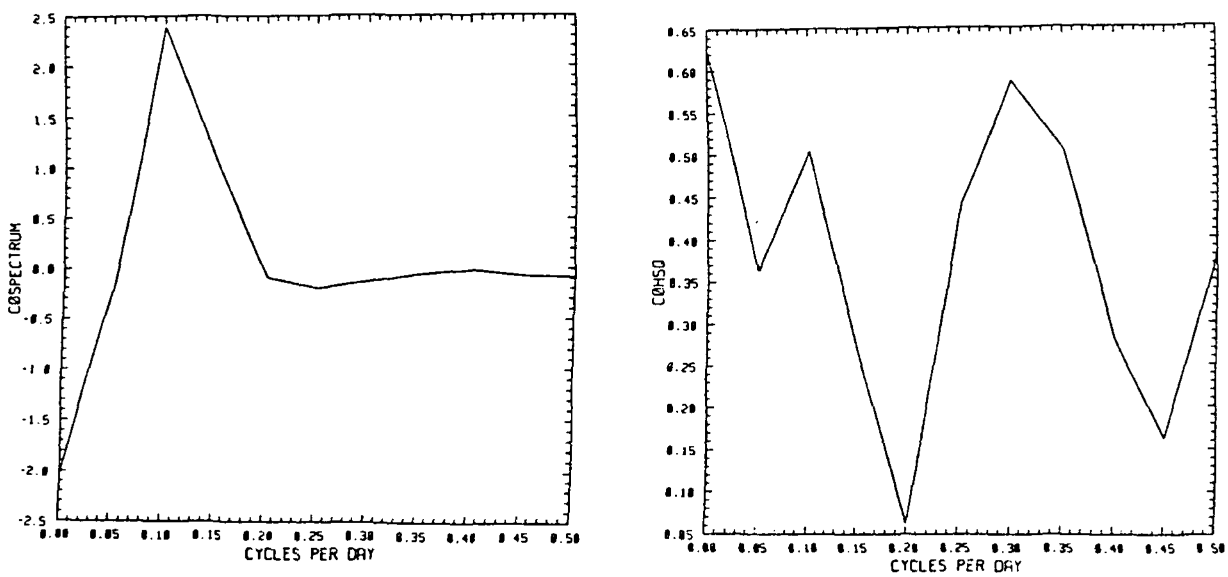

Fig. 31. Cross spectrum analysis for $\partial u/\partial t$ vs wave forcing, 50 to 500 mb, 60^{o}N to 82^{o}N for FGGE data

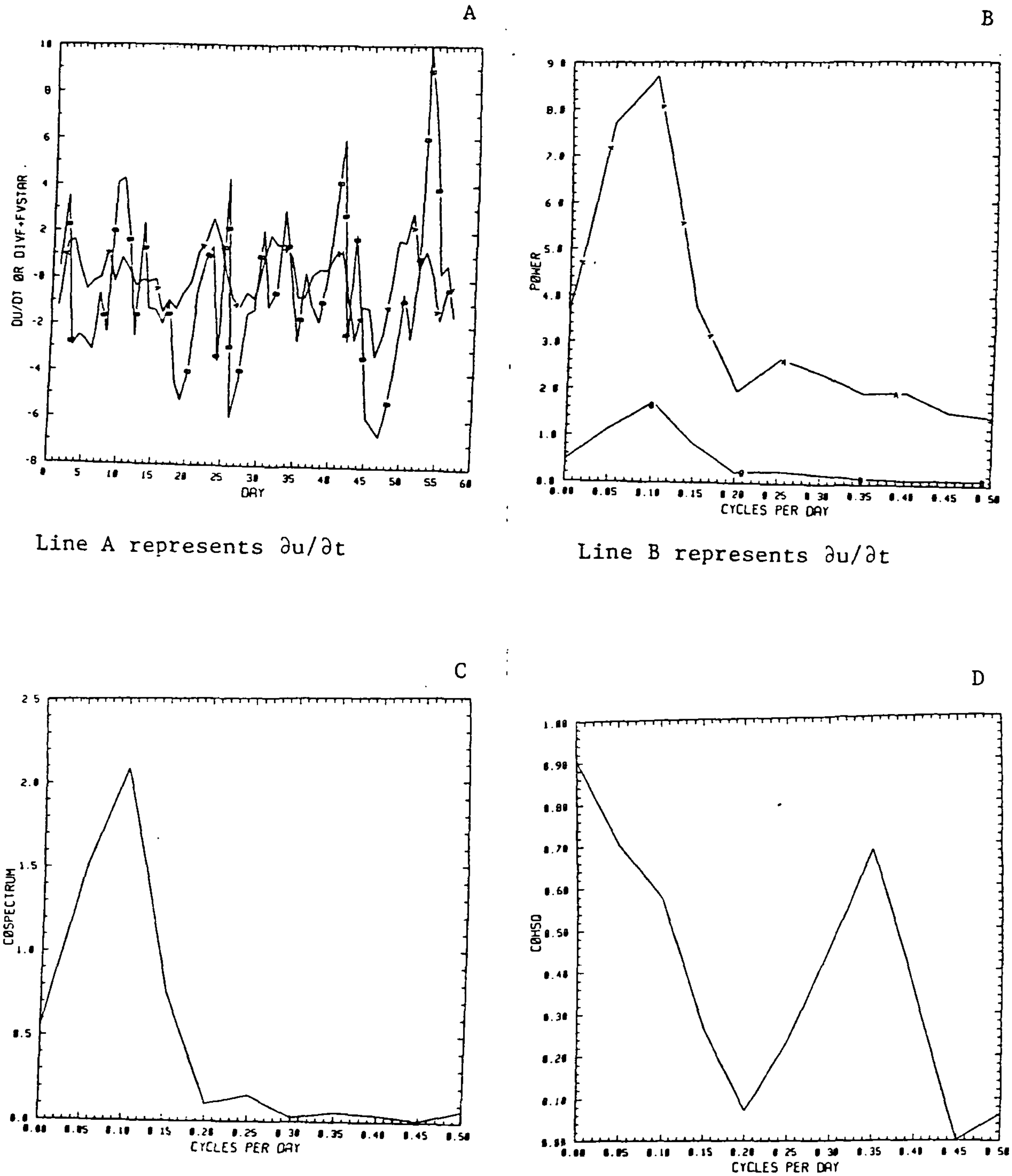

Fig. 32. Cross spectrum analysis for $\partial u/\partial t$ vs wave forcing + $f\bar{v}*$, 50 to 500 mb, 60^oN to 82^oN for FGGE data

A close examination reveals the Fig. 30 lacks many well correlated regions. The region picked was one of large divergence, so in effect it is a "worst case" (i.e., most of the wave driving was known a priori not to force mean flow changes). Changes in the mean flow are small, and differences between the two larger terms puts the mean flow change in the "noise" range.

The same analysis was performed for the region 500-50 mb and 60-83°N. This is the region that experienced the two wave activity events near days 20 and 50. These events are very clear in Figure 30a. It is also clear that during these events the mean flow tended to increase: During these two periods, mean flow changes of about 2 ms^{-1} day^{-1} occurred. The correlation coefficient for $\partial u/\partial t$ vs. wave driving was calculated to be only .077. The cospectrum indicates that all of the positive contribution to this relationship comes from oscillations with periods of about a week. Again, the coherence squared is erratic, and is not consistent with Figure 29d.

Including the $f\bar{v}^*$ term, the correlation coefficient was .382. From Figure 32a, it is apparent that the residual circulation compensates a great deal for the wave driving. Another was of viewing this is that the term $\frac{\partial}{\partial p}(\overline{v'\theta'}/\bar{\theta}_p)$ is the largest part of the EP flux divergence. It is automatically compensated for in

$$(20)\quad f\bar{v}^* = f\bar{v} - f\frac{\partial}{\partial p}(\overline{v'\theta'}/\bar{\theta}_p)$$

It is possible that the reason for low correlation coefficients is the noisy pattern of $\nabla\cdot\mathbf{F}$. The small scale intense regions of

divergence and convergence that can be seen in the daily EP diagrams (Figs. 17 and 18) is mainly the result of taking special derivatives of noisy heat and momentum flux fields.

5. GLAS Model Results

a) Zonal mean fields

As in the case of the FGGE data, we here compare the GLAS data with Oort's general circulation climatology. (The figures from Oort (1983) corresponding to those for the GLAS model data are located with the corresponding FGGE data figures). The zonal mean zonal wind component (Fig. 33a) differs from the climatological field (Fig. 2a). The jet in the northern hemisphere is about 10 ms^{-1} too strong and it is located about 10° too far north, at about 40°N.

Another unusual feature of this jet is that it has a maximum at 100 mb at the top of the model (this is a common deficiency in GCM's with top boundaries in the lower stratosphere), while the jet in the real atmosphere has a maximum at about 200 mb. A series of five-day mean are shown. These diagrams show how the abnormal jet developed over time.

Figures 34-36 show the development of the northern hemisphere GLAS model jet. Initially, the wind field was quite reasonable because the model was initialized with real atmospheric data. But as the model lost its memory of the initialization, the jet moved northward, increased its speed and its core moved to the top of the

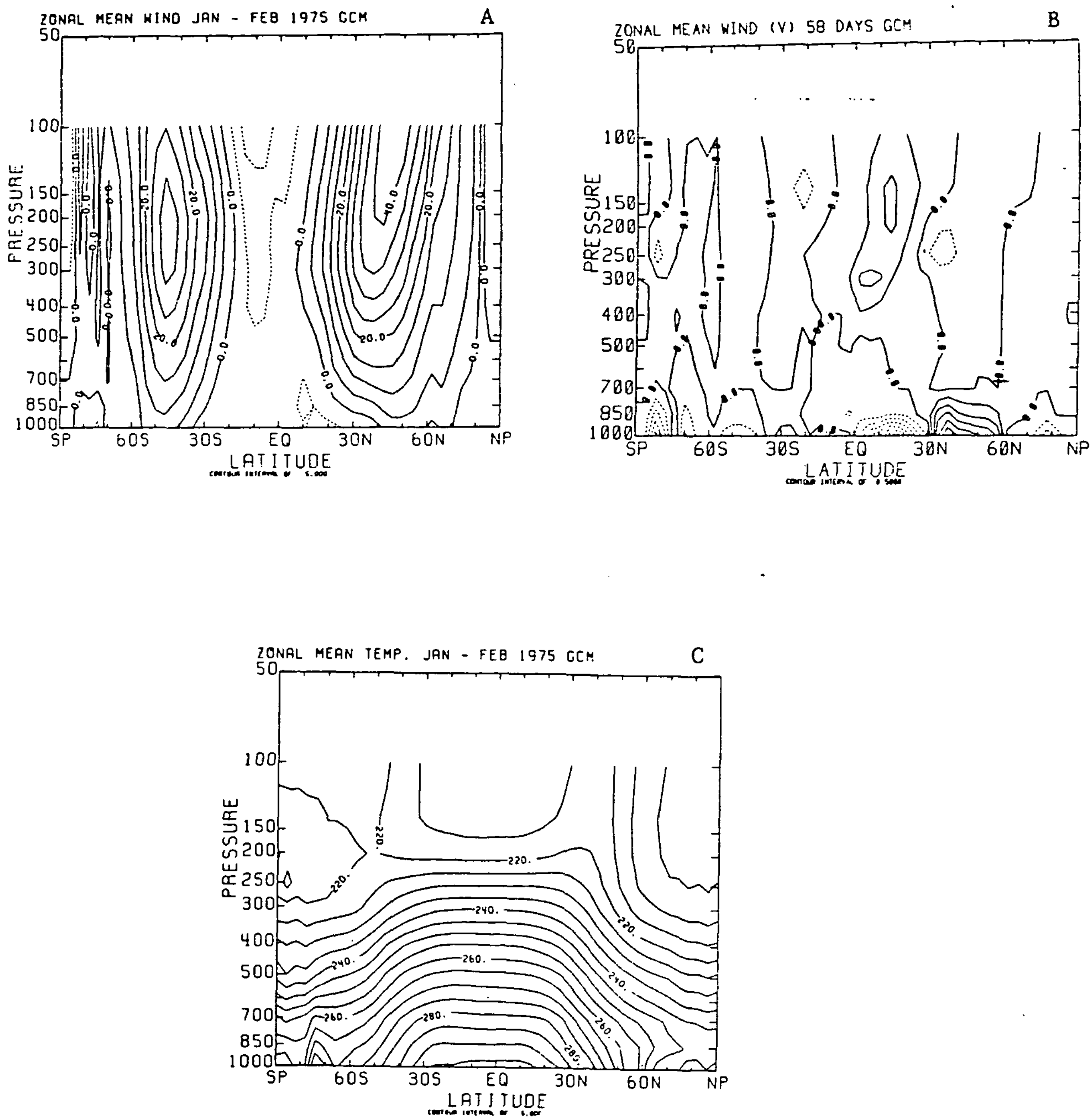

Fig. 33. Zonal mean zonal and meridional wind components and temperature for GLAS model. The contour interval for 33B is .5 ms^{-1}

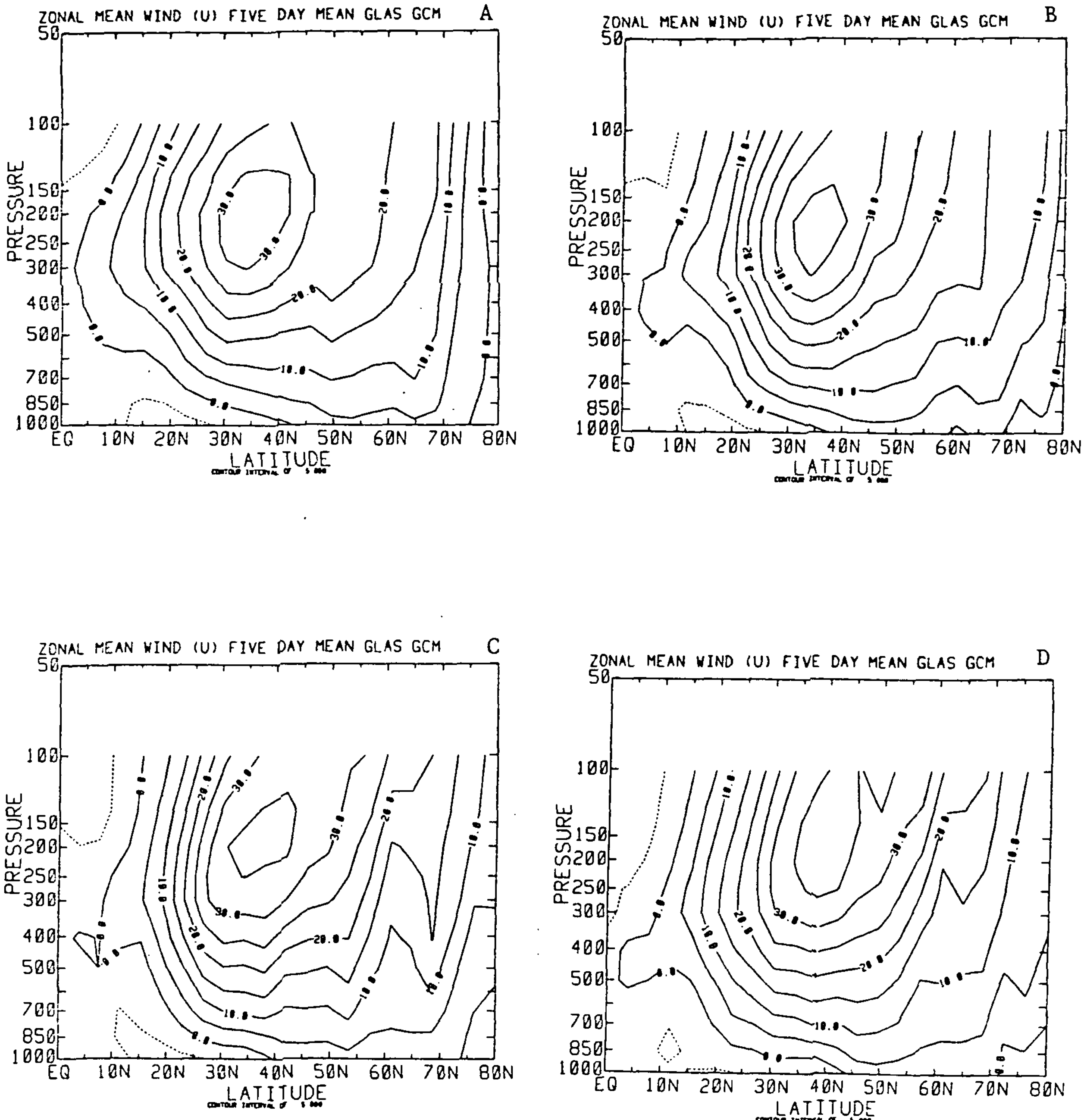

Fig. 34. 5-day means of zonal wind component in GLAS model

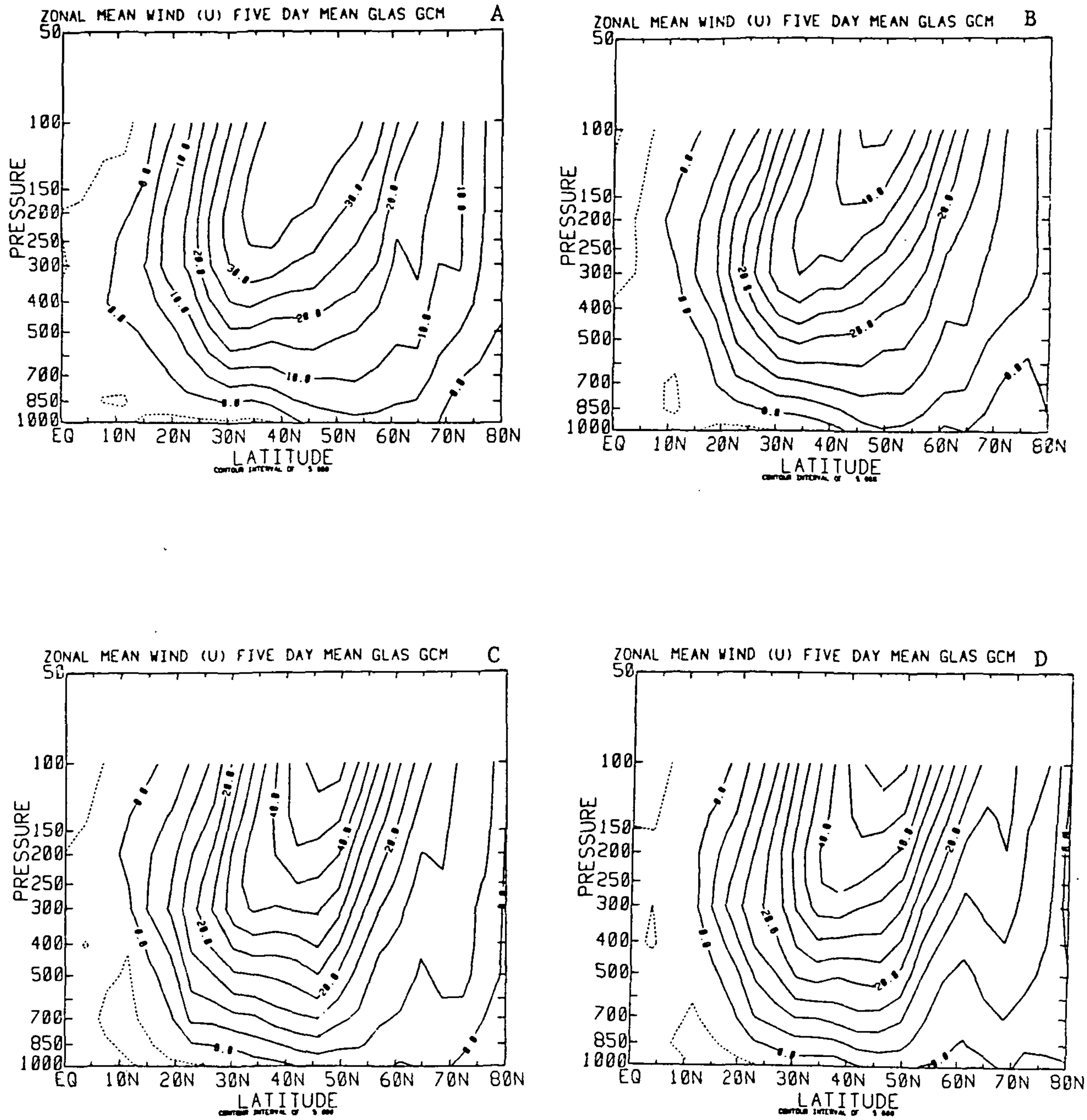

Fig. 35. 35-day means of zonal wind component in GLAS model

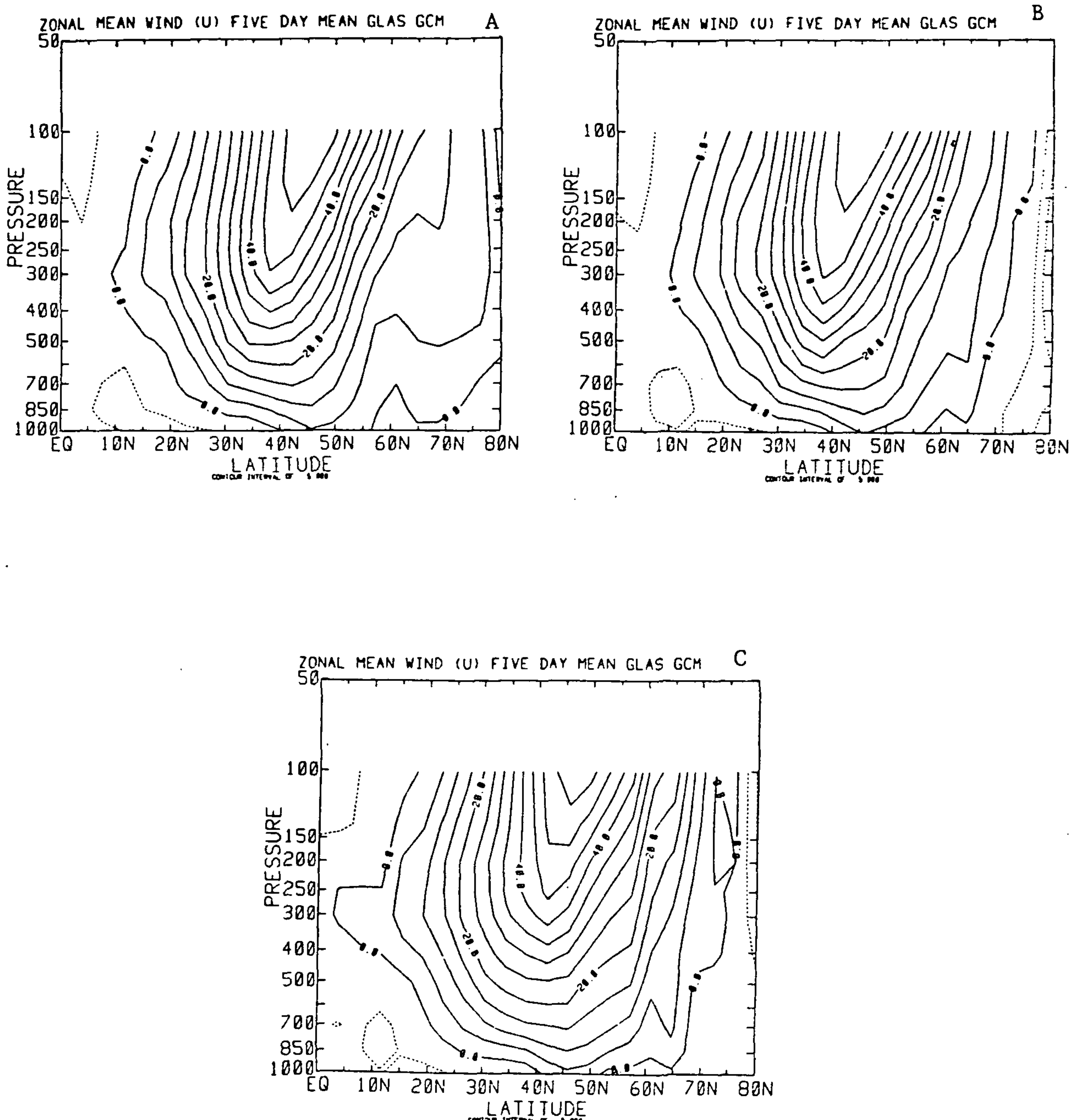

Fig. 36. 5-day means of zonal wind components in GLAS model

model. This behavior may be at least partially explained by vertically propagating planetary waves interacting with the "lid" of the model, rather than propagating higher into the stratosphere. This is a significant fault of the model.

In a similar model, Hansen et al. (1983) found that they could eliminate this problem by either moving the lid to a much higher level or by including damping at the top of the model.

Figure 33b shows the zonal mean meridional wind component. The Hadley cell circulation is evident, but the maximum wind speed in the lower stratosphere is only about one third of that in the real atmosphere. The Ferrel cell circulation is also present and its circulation appears to be too strong below 850 mb.

The main features of the meridional wind are simulated, but strengths of the circulation cells does not agree well with the Oort climatology.

The zonal mean temperature (Figure 33c) is a reasonable simulation of the real atmosphere. The lower stratosphere is 10°-15°C too warm but the overall structure is good.

One unusual feature is the strong north-south temperature gradients poleward of 30° in both hemispheres. The transition from the tropics to the high latitudes is smoother in the real atmosphere (Figure 4a).

The northward momentum transport by transient eddies (Figure 37a) is similar in overall appearance to the Oort data (Figure 6a) but has several significant differences. In the southern hemisphere there is an unusual maximum south of 70°S and about 150 mb.

In the northern hemisphere, the maximum at 30°-35° is well simulated, but farther to the north there is a large equatorward transport with strong north-south gradients that does not appear in the Oort data set.

The simulation of the northward transport of momentum by the stationary waves (Figure 37b) is not nearly as successful. As with the transient eddies, in the southern hemisphere there is an anomalous maximum south of 70°S.

In the northern hemisphere, there is a large amplitude negative region in the mid-latitudes below 700 mb that is not seen in the Oort data set. The maximum at 300 mb, 30°N that is clearly seen in the Oort data set is much too weak in the model, as is the negative region north of 50°N.

The northward transport of heat by transient eddies is shown in Figure 38a. In the southern hemisphere, the large negative region in the lower troposphere has its maximum at 1000 mb, unlike the atmospheric data (Figure 7a). The negative region at about 200 mb and 50°S is similar to the Oort data, but the large, weak positive region between 400-500 mb does not appear in the model data.

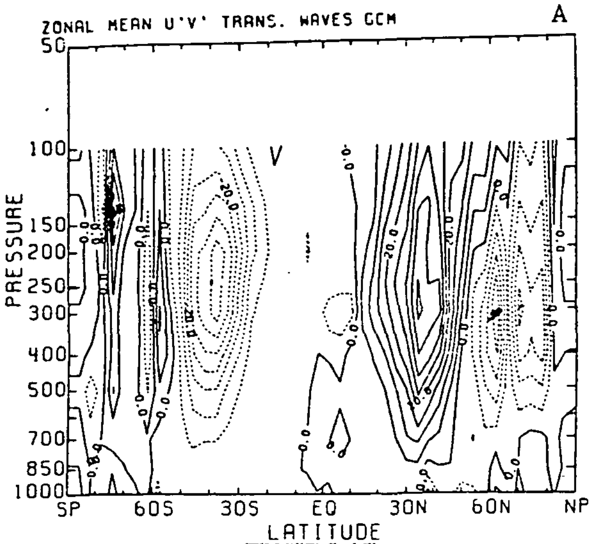

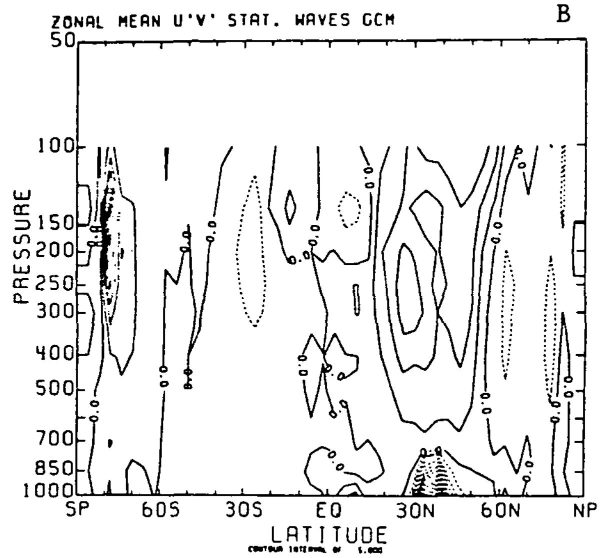

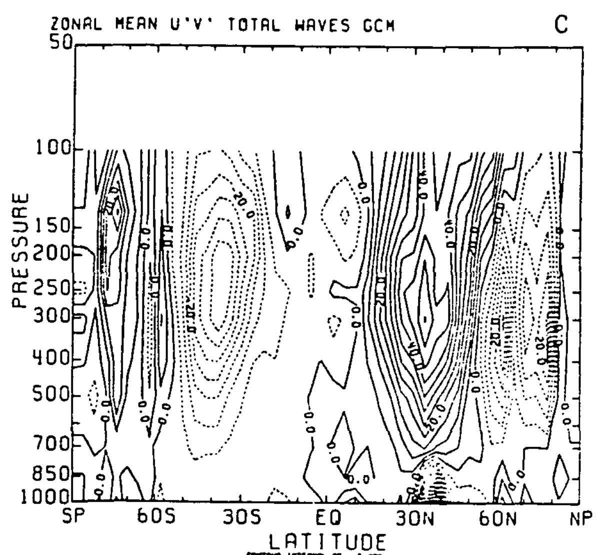

Fig. 37. Zonal mean northward transport of momentum by transienct, stationary and total waves in GLAS model. The contour interval is 5 m^2s^{-2}

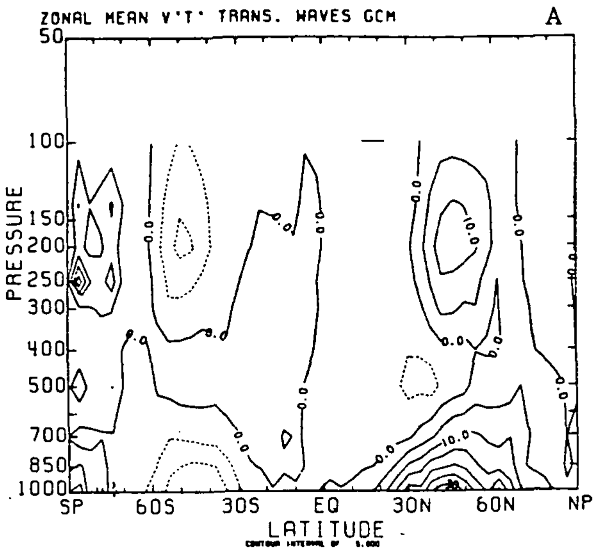

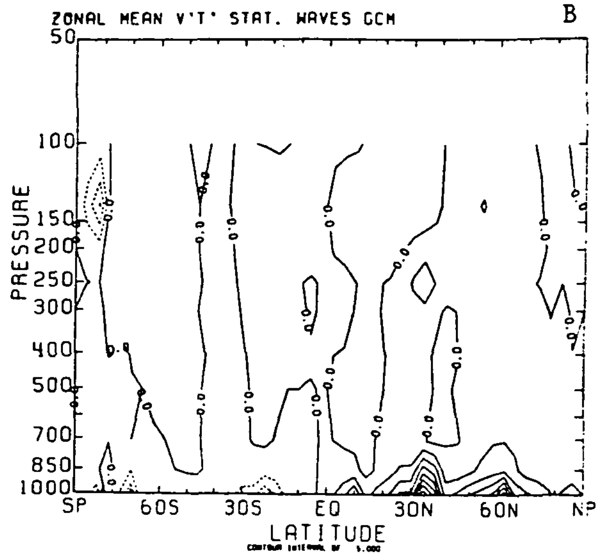

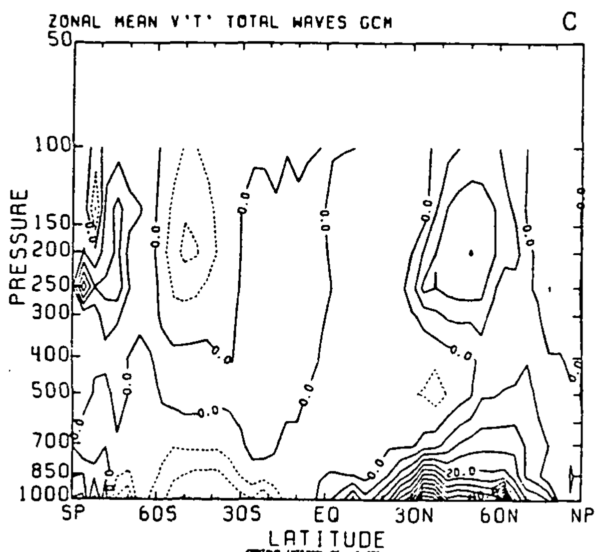

Fig. 38. Zonal mean northward transport of heat by transient, stationary and total waves in GLAS model. The contour interval is 5 ms^{-1}°C

The northern hemisphere lower tropospheric maximum is much too strong and extends too low. The maximum at about 200 mb is also too strong.

Although the same gross features are found in the Oort data, the model differs significantly from the atmosphere in its heat transport by transient eddies, especially in the lower troposphere.

The northward transport of heat by stationary waves (Figure 38b) differs even more from the Oort climatology than does the transient flux. There are several small minima at 1000 mb in the southern hemisphere in the model, but overall, the field is weak.

The expected large maximum region north of 30°N is reproduced only in the lowest part of the troposphere. This is very different from the Oort data.

In the atmosphere, there is a large northward heat transport throughout the 50-1000 mb region. Even near 1000 mb, where the maxima are similar, the vertical gradients are opposite due the model producing the largest value near the ground.

Figure 39 shows streamfunctions for the mean meridional circulation and the residual circulation. The Hadley circulation is weak. The Ferrel cell is also weak. The apparent strong meridional flow below 850 mb in mid-latitudes may be partly an artifice of the finite differencing procedure in integrating downward from 100 mb.

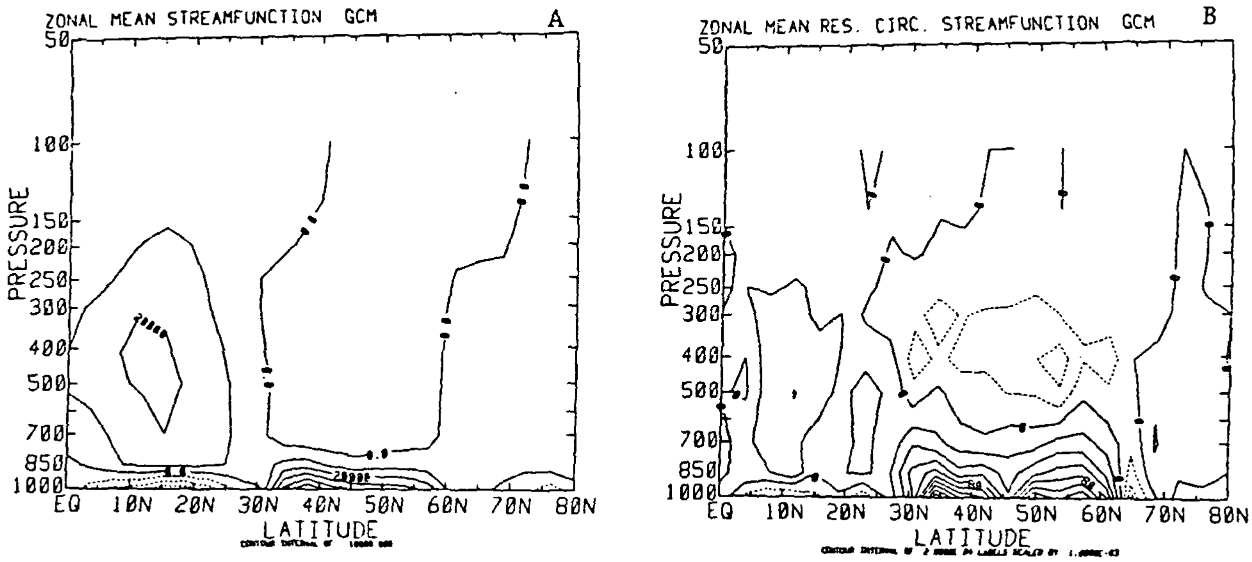

Fig. 39. Zonal mean streamfunction for the mean meridional circulation and residual circulation streamfunction for GLAS model

The residual circulation has some of the gross features of Figure 6a in Edmon et al. (1980). However, the unusual heat flux pattern below 850 mb results in unusual residual circulation there in mid-latitudes.

b) Eliassen-Palm diagrams

The EP flux and EP flux divergence for the transient waves are shown in Figure 40a. There are two main differences between the model and the Oort data (Figure 18b).

One is that the amplitude of the divergence is too great. This is due to the gradients of both the heat and momentum fluxes being too large.

The other more serious problem is that the model totally misses the divergence below 700 mb and puts a maximum in convergence down to 1000 mb. This is because, in the model, the maximum heat flux occurs at 1000 mb, which reverses the vertical gradient.

Aside from the lower troposphere, the model does reproduce the main features found in the Oort data set. The pattern of EP flux is qualitatively correct and the positive and negative regions match fairly well.

The EP flux diagram for stationary waves is similar in that it does not show the divergence in the lower troposphere (Figure 40b) for the same reason as the transient waves. The simulation above 500 mb is fairly good.

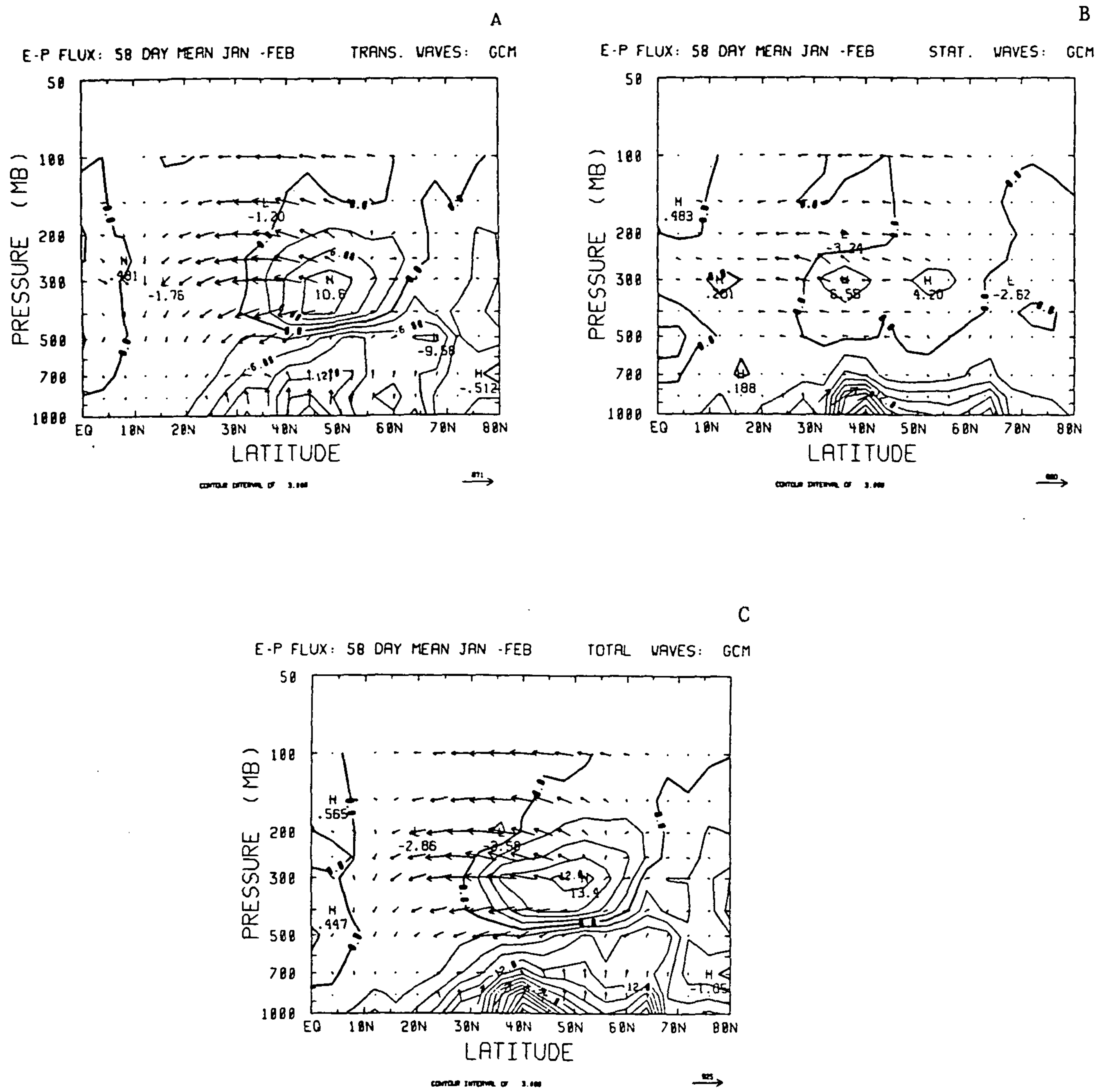

Fig. 40. Eliassen-Palm diagrams for transient, stationary and total waves in the GLAS model. The contour interval is 3 ms^{-1} day $^{-1}$

The total wave EP flux, of course, suffers from the lack of divergence in the lower troposphere. In general, the magnitude of the divergence is about twice that of the Oort data. Above 500 mb, the simulation is reasonable, but below 700 mb, the pattern is nearly opposite to that of Oort data.

As with the FGGE data, a series of consecutive five-day means for transient waves were calculated. These are shown as Figures 41-43. This series does not have any events as spectacular as those of the FGGE series. However, there are some interesting changes and developments.

The period up to day 24 was rather uneventful, but from day 25-29 a large southward momentum flux occurred above 500 mb, north of 50°N but disappeared before the next period. A similar event occurred from day 40-49.

Throughout the entire period, the main areas of convergence and divergence remained in the same general locations but varied somewhat in amplitude. There were also numerous convergent events below 200 mb.

c) Cross Spectral Analysis

The same time series analysis that was done for the FGGE data was done for the model data. The region used was 36°N to 60°N, from 200 mb to 500 mb.

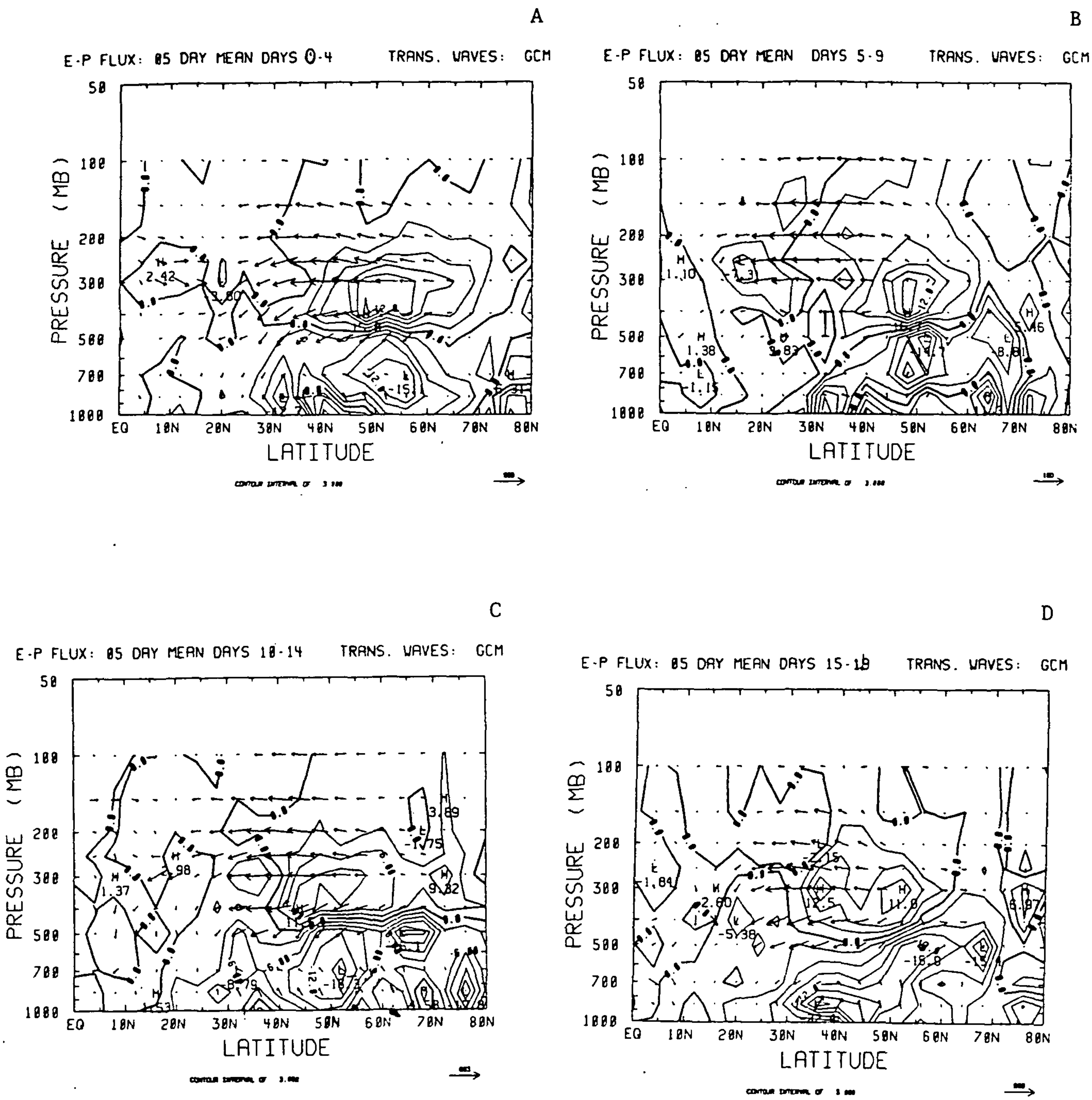

Fig. 41. 5-day means of transient wave Eliassen-Palm flux in GLAS model

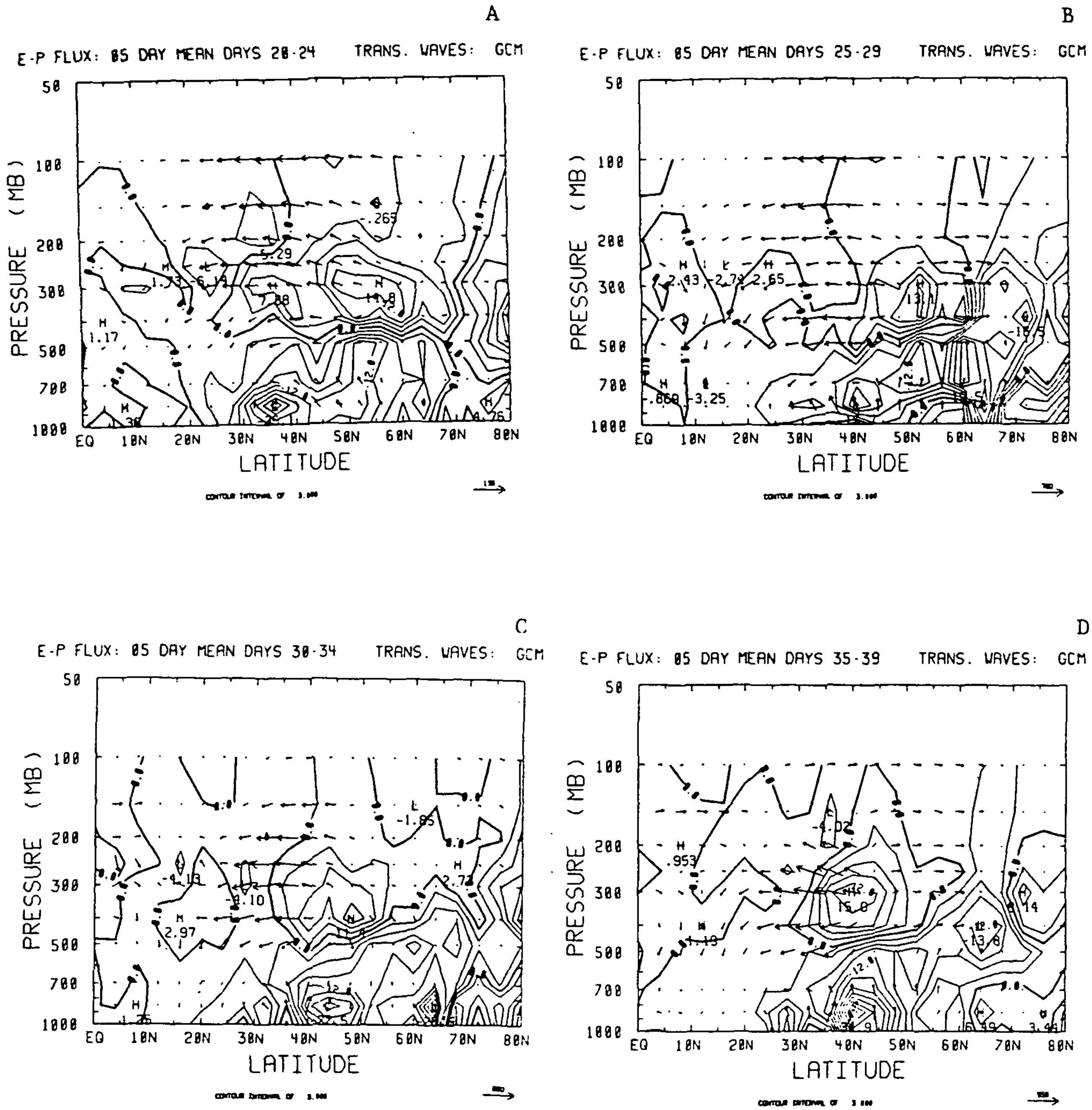

Fig. 42. 5-day means of transient wave Eliassen-Palm flux in GLAS model

A

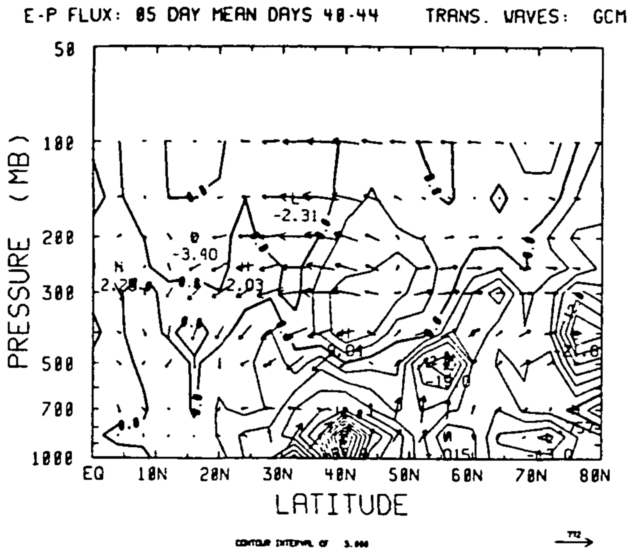

B

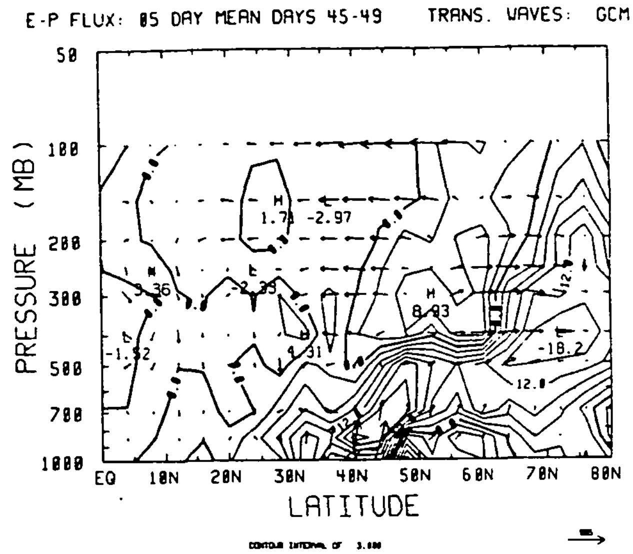

C

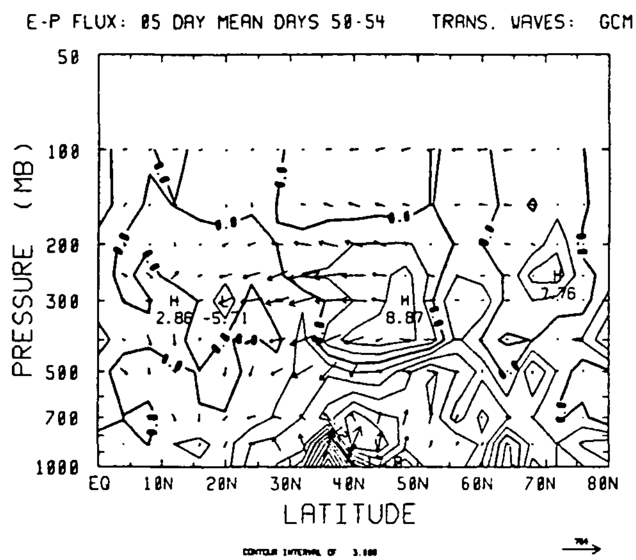

Fig. 43. 5-day means of transient wave Eliassen-Palm flux in GLAS model

The time series for $\partial u/\partial t$ vs. wave driving, Figure 44a, had a correlation coefficient of .308, considerably higher than that for the FGGE data. Most of the cross covariance came from oscillations with periods of a week or more. The values of coherence are fairly low but indicate that the best relationship between the variables is for periods from 3 days to a week.

Figure 44 shows results of the same analysis, but including the residual circulation term $f\bar{v}^*$. The correlation coefficient was .487, indicating that $f\bar{v}^*$ does compensate for the wave driving. Most of the cross covariance is due to oscillations with periods of about 5-7 days. This is not similar to the equivalent figure for the FGGE data.

6. Concluding Remarks

The FGGE data is for a period of time that was fairly typical of climatology. Most of the zonal mean fields are very similar to the Oort climatology.

The model data differs from the atmospheric data too much to make extensive useful comparisons. The northern hemisphere jet is too strong, too high and too far north. The northward heat fluxes are a maximum at the ground, which is a feature found in neither the FGGE nor the Oort data.

Hansen et al. presented EP fluxes for a similar model for January. This is shown as Figure 46. This figure can be compared with Figure 18a, for the FGGE data and Figure 39c for the GLAS model data. Although the plotting convention of Hansen et al. is different, the location of areas of convergence and divergence can be compared.

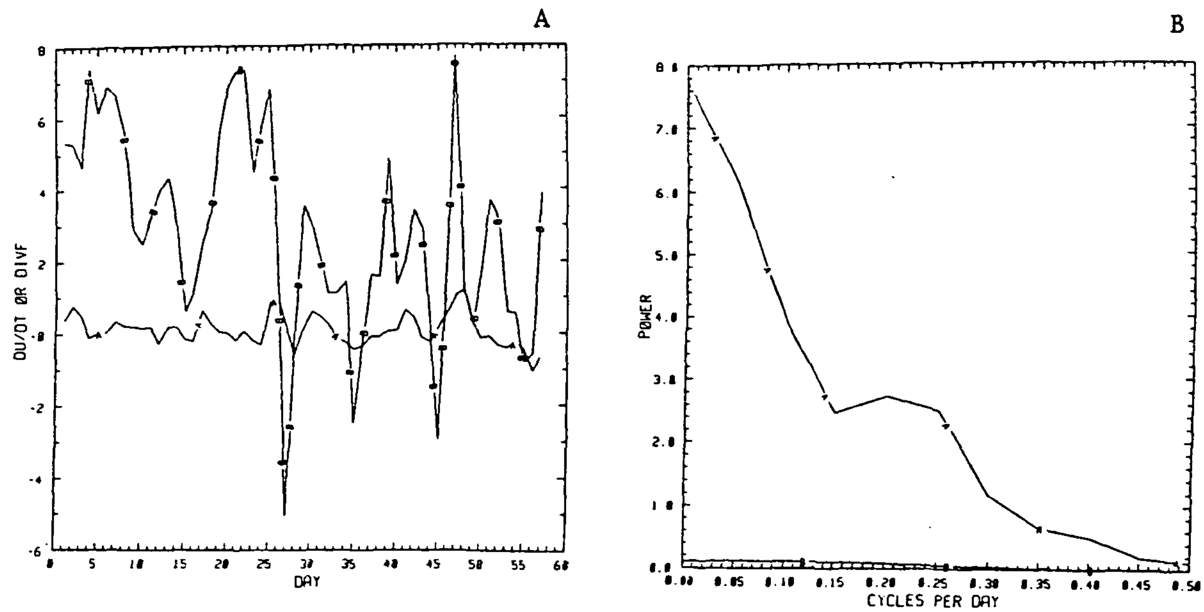

Line A represents $\partial u/\partial t$

Line B represents $\partial u/\partial t$

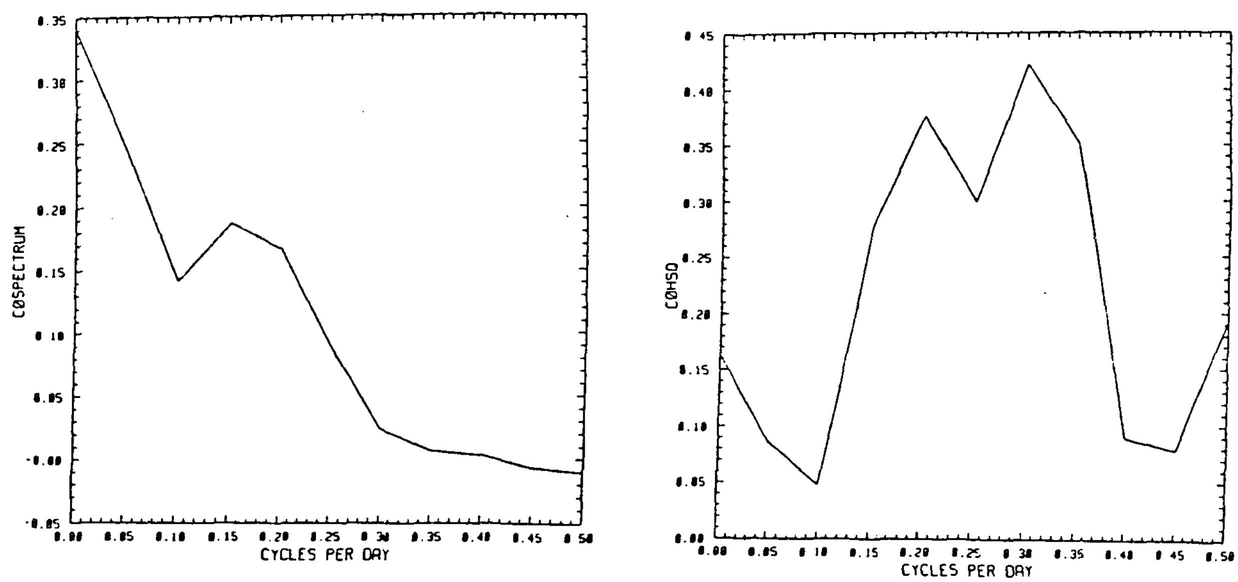

Fig. 44. Cross spectrum analysis for $\partial u/\partial t$ vs wave driving. 200 to 500 mb, 36°N to 60°N, in the GLAS model

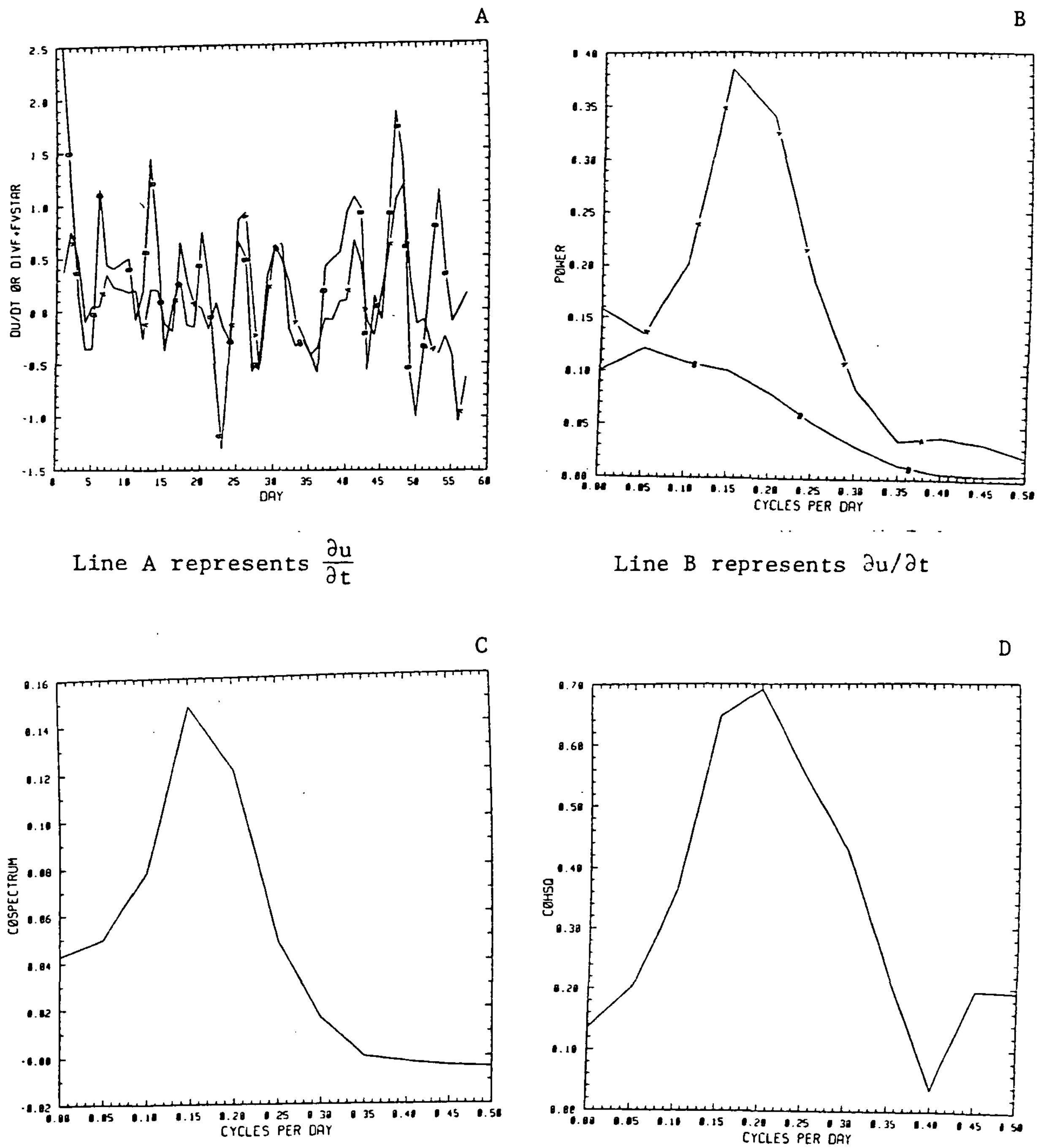

Fig. 45. Cross spectral analysis for $\partial u/\partial t$ vs wave driving + $f\bar{v}^*$, 200 to 500 mb, 36°N to 60°N, in the GLAS model

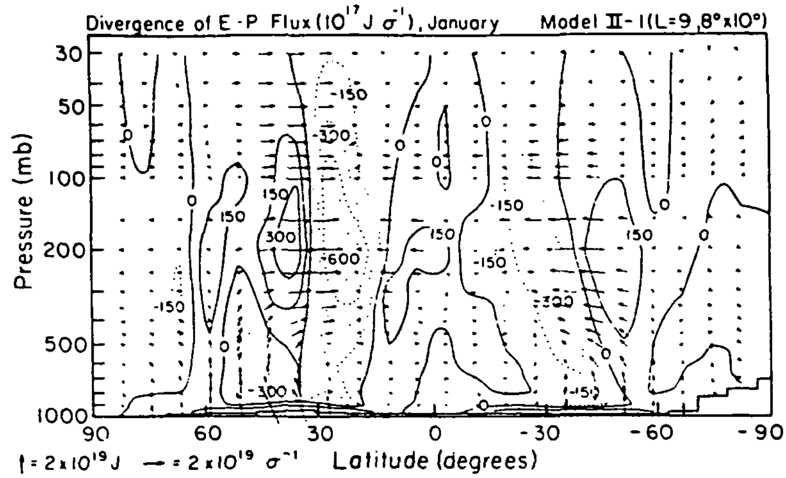

Fig. 46. Eliassen-Palm diagram for the Hansen et al model in January. (From Hansen et al, 1983)

The Hansen et al. model does reproduce the divergence in the lower troposphere. The pattern of arrows is similar to both the FGGE and the GLAS model data. The Hansen et al. model has a strongly convergent region just south of 30°N, with a maximum near 200 mb. Although this feature is found in the GLAS model and the Oort data, it is much weaker. The feature is caused by strongly divergent momentum fluxes.

The Hansen et al. model simulates the real atmosphere and the FGGE data set more closely than the GLAS model.

The GLAS model data is less noisy than the FGGE data for day-to-day calculations. This data set may be more useful for spectral analysis since the wave forcing is more closely related to changes in the mean flow.

For most investigations, the FGGE data set would be better, if only because the GLAS model does not adequately simulate the lower troposphere. Use of a short period simulation from the GLAS model, which has been initialized with real data, as in the model run used here, cannot be recommended. The "climate drift" of the model (i.e. the temporal change of the mean zonal wind from the initial state to the model "climate" mean) is simply too large. Partitioning the eddy statistics between transient and stationary eddies may be misleading during the "drift" phase of the model. Further EP studies with the GLAS model or other GCM's should be done using long time histories in which the effect of initial conditions can be minimized.

REFERENCES

Andrews, D. G., and M. E. McIntyre, 1976: Planetary waves in horizontal and vertical shear: the generalized Eliasson-Palm relation and the mean zonal acceleration. J. Atmos. Sci., 33, 2031-2048.

Andrews, D. G. and M. E. McIntyre, 1978: Generalized Eliassen-Palm and Charney-Drazin theorems for waves on axisymmetric flows in compressible atmospheres. J. Atmos. Sci., 35, 175-185.

Charney, J. G., and P. G. Drazin, 1961: Propagation of planetary-scale disturbances from the lower into the upper atmosphere. J. Geophys. Res., 66, 83-109.

Dunkerton, T., C.-P. F. Hsu and M. E. McIntyre, 1981: Some Eulerian and Lagrangian diagnostics for a model stratospheric warming. J. Atmos. Sci. 38, 819-843.

Edmon, H. J., B. J. Hoskins and M. E. McIntyre, 1980: Eliassen-Palm cross sections for the troposphere. J. Atmos. Sci., 37, 2600-2616.

Hartmann, D. L., C. P. Mechoso and K. Yamakazi, 1984: Observations of wave-mean flow interactions in the southern hemisphere. J. Atmos. Sci., (in press)

Holton, J. R., 1975: The Dynamic Meteorology of the Stratosphere and the Mesosphere. Meteor. Monogr., No. 37, Amer. Meteor. Soc., 218 pp.

Hoskins, B. J., 1983: Modeling of transient eddies and their feedback onto the mean flow. In "Large-scale Dynamical Processes in the Atmosphere." Academic Press, 1983.

Oort, A. H., 1983: Global Atmospheric Circulation Statistics, 1958-1973. NOAA Prof. Pap. 14, U.S. Dept. of Commerce, Washington, D.C., 180 pp.

Oort, A. H. and E. M. Rasmusson, 1971: Atmospheric circulation statistics. NOAA Prof. Pap. 5, U.S. Dept. of Commerce, Washington, D.C., 323 pp.

Palmer, T. N., 1981: Diagnostic study of a wavenumber - 2 stratospheric sudden warming in a transformed Eulerian - mean formalism. J. Atmos. Sci., 38, 844-855.

Palmer, T. N., 1982: Properties of the Eliassen-Palm flux for planetary scale motions. J. Atmos. Sci., 39, 992-997.

Stone, D. H., and G. Salustri, 1984: Generalization of the Eliassen-Palm flux to include eddy forcing of condensation heating. J. Atmos. Sci., (in press).

Strauss, D. M., 1983: Conservation laws of wave action and potential vorticity for Rossby waves in a stratified atmosphere. NASA Technical Memorandum 86058.